Journal of Palaeogeography, 2022, 11(2): 151—172 (00262)

Available online at www.sciencedirect.com

ScienceDirect

journal homepage: http://www.journals.elsevier.com/journal-of-palaeogeography/

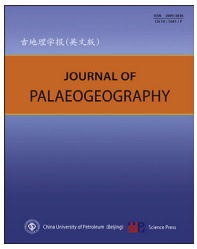

Lithofacies palaeogeography and sedimentology

The primary dolostone in the Meso-Neoproterozoic: Cases study on platforms in China

Zhi-Dong Bao [a,b,*], *Han-Cheng Ji* [a,b], *Yuan Wang* [a], *Zong-Feng Li* [a], *Ting Liang* [a,b], *Bo Niu* [a,b], *Ming-Yang Wei* [a], *Kai Lu* [a], *Yan-Qing Shi* [a,b], *Hua Zhang* [a], *Pu Wan* [a], *Zhuo-Lun Li* [a], *Zhi-Bo Yang* [a], *Rui Liu* [a], *Can-Xing Liu* [a], *Xu-Lin Zhong* [a], *Xiao-Qi Guo* [a], *Peng-Fei Xiang* [a], *Zhong-Xian Cai* [c], *Shui-Chang Zhang* [d]

[a] *China University of Petroleum (Beijing), Beijing 102249, China*
[b] *State Key Laboratory of Petroleum Resources and Prospecting, Ministry of Education, Beijing 102249, China*
[c] *China University of Geosciences (Wuhan), Wuhan 430074, China*
[d] *PetroChina Research Institute of Petroleum Exploration and Development, Beijing 100083, China*

Abstract Meso-Neoproterozoic dolostone is abnormally well-developed in the platform areas in China, detailly, in the Mesoproterozoic Calymmian Wumishan Formation of North China Basin, Neoproterozoic Ediacaran Qigbulak Formation of Tarim Basin, and the Neoproterozoic Ediacaran Dengying Formation of Sichuan Basin. The outcrops and drilling cores from these basins show that these dolostones are mostly thick-bedded to massive, with mud-sized to silt-sized crystalline dolostone reaching 86%—97% of the total dolostone thickness. These dolostones basically suffered no secondary metasomatism, regardless of containing microorganisms (such as algae and bacteria) or not. The analyses of sedimentary palaeogeographic features indicate that: (1) the Meso-Neoproterozoic dolostone nearly covered the entire area basins, and was widely deposited in supratidal to intertidal zones, as well as in open platform environments; (2) the dolostone was subdivided according to the crystalline size, with the distribution controlled by geomorphology, i.e., the pure mud-sized crystalline dolostone developing in depression areas, whereas the grainy mud-sized crystalline dolostone or the mound stromatolitic mud-sized crystalline dolostone developing in uplift areas; (3) deep-water basins developed between the carbonate platforms, and the seismic profiles show that these basins were formed by syngenetic deep faults in the Meso-Neoproterozoic strata. These syngenetic faults increased Mg^{2+} concentration in the seawater by injecting rich-Mg^{2+}-bearing hydrothermal fluids into the carbonate platforms. The analyses of geochemical and paleoclimatic indexes reveal that there is no obvious difference in carbon and oxygen isotope ratios between dolostones having different textures, with the ratios similar to those of the global seawater of the Meso-Neoproterozoic, indicating that the silt-sized crystalline dolostone has the same sedimentary origin as the mud-sized crystalline dolostone, i.e., the former is from authigenic recrystallization

* Corresponding author. China University of Petroleum (Beijing), Beijing 102249, China.
E-mail address: baozhd@cup.edu.cn (Z.-D. Bao).
Peer review under responsibility of China University of Petroleum (Beijing).
https://doi.org/10.1016/j.jop.2022.03.001

of the latter rather than secondary metasomatism. Therefore, whatever the crystalline sizes are, the dolostones are all originated from sedimentation. All the petrological, sedimentary and geochemical data suggest that the dolostones covering almost the whole Meso-Neoproterozoic typical platform areas of China are of relatively primary sedimentary origin.

Keywords Thick-bedded to massive dolostone, C—O isotopes, Meso-Neoproterozoic, Tarim basin, Sichuan basin, North China Basin

Received 26 December 2021; revised 23 February 2022; accepted 24 February 2022; available online 5 April 2022

1. Introduction

The carbonate rocks around the world are dominated by limestones in the Phanerozoic and dolostones in the pre-Phanerozoic (Tucker, 1982; Sun, 1994; Feng *et al.*, 2004). Since the Phanerozoic, most of the dolostones are post-penecontemporaneous, of secondary metasomatism genesis, and show fine-to medium-grained, or saccharoidal crystalline texture; while only a small amount are penecontemporaneous, showing mainly oxidated colors and occasionally reduced colors. These penecontemporaneous dolostones are mainly thin-bedded, mud-to silt-sized, and contain more terrigenous impurities such as clay minerals and quartz grains. They are relatively tight, and can serve as seals for oil and gas reservoirs. Comparatively, post-penecontemporaneous dolostones are relatively well-developed with intercrystalline and other types of pores during diagenetic processes (e.g., dolomitization), and therefore often become favorable reservoirs for hydrocarbon accumulation (de Dolomieu, 1791; Zhao *et al.*, 1977; Zenger *et al.*, 1980; Mountjoy and Halim-Dihardja, 1991; Feng *et al.*, 1992; Bao, 1998, 1999; Bao *et al.*, 1998, 1999a, 1999b, 2004, 2006, 2007; Jin and Feng, 1999; Warren, 2000; Zhao and Zhu, 2001; Wei *et al.*, 2006; He *et al.*, 2010; Huang, 2010; Zhu *et al.*, 2013; Zhang *et al.*, 2014; Wang, 2017; Yang *et al.*, 2017).

In recent years, the Proterozoic strata, which are buried deep to ultra-deep (i.e., below 6000 m or even 6500 m), have gradually attracted the attention of geoscientists all over the world. Previous studies show that the Proterozoic strata, especially the Meso-Neoproterozoic strata, developed extremely-thick carbonate rocks, in which a large number of dolostones are widely distributed in the sedimentary basins globally. These dolostones show abnormal development of sedimentary thicknesses and crystal texture, indicating a genesis different from that of the Phanerozoic dolostones (Pratt, 2001; Turner, 2009; Zhu, 2016).

2. Developments of Meso-Neoproterozoic dolostone in the platforms in China

Tarim Basin, North China Basin, and Sichuan Basin, as platform sedimentary areas in China, have deposited more than 10,000 m thick carbonate rocks since the Proterozoic. The Meso-Neoproterozoic dolostones in these three platforms are of great thickness and have distinct sedimentary characteristics.

2.1. Measurements of the outcrops

In this study, 23 Meso-Neoproterozoic outcrops and wells have been measured (Fig. 1), i.e., 4 outcrops and 4 wells in Tarim Basin, 3 outcrops and 6 wells in North China Basin, and 2 outcrops and 4 wells in Sichuan Basin, respectively. As shown in the outcrops and the drilling cores, the lithology is dominated by dolostone, especially medium-thick bedded to massive (Table 1) mud-sized or fine crystalline dolostone.

2.1.1. Shiazik section of Tarim Basin

The thickness of Upper Ediacaran Qigbulak Formation in Shiazik section, Tarim Basin, is 164.50 m and mainly composed of the medium-thick bedded dolostone, which can be divided into three lithological members (Fig. 2). It overlies the Upper Ediacaran Sugaitebulak Formation, which is dominated by red littoral facies clastic rocks.

The thickness of Member I of the Qigbulak Formation is 18 m. At the bottom are massive siltstones with a thin layer (30 cm thick) of oolitic dolostone, and the argillaceous content in upward siltstone increases and the thickness decreases to less than 20 cm. From the thin-layer of the argillaceous siltstone upward, the laminar dolostone gradually evolved from the thin-layer to the medium-thick layer and the cabbage-shaped stromatolites are developed at the top.

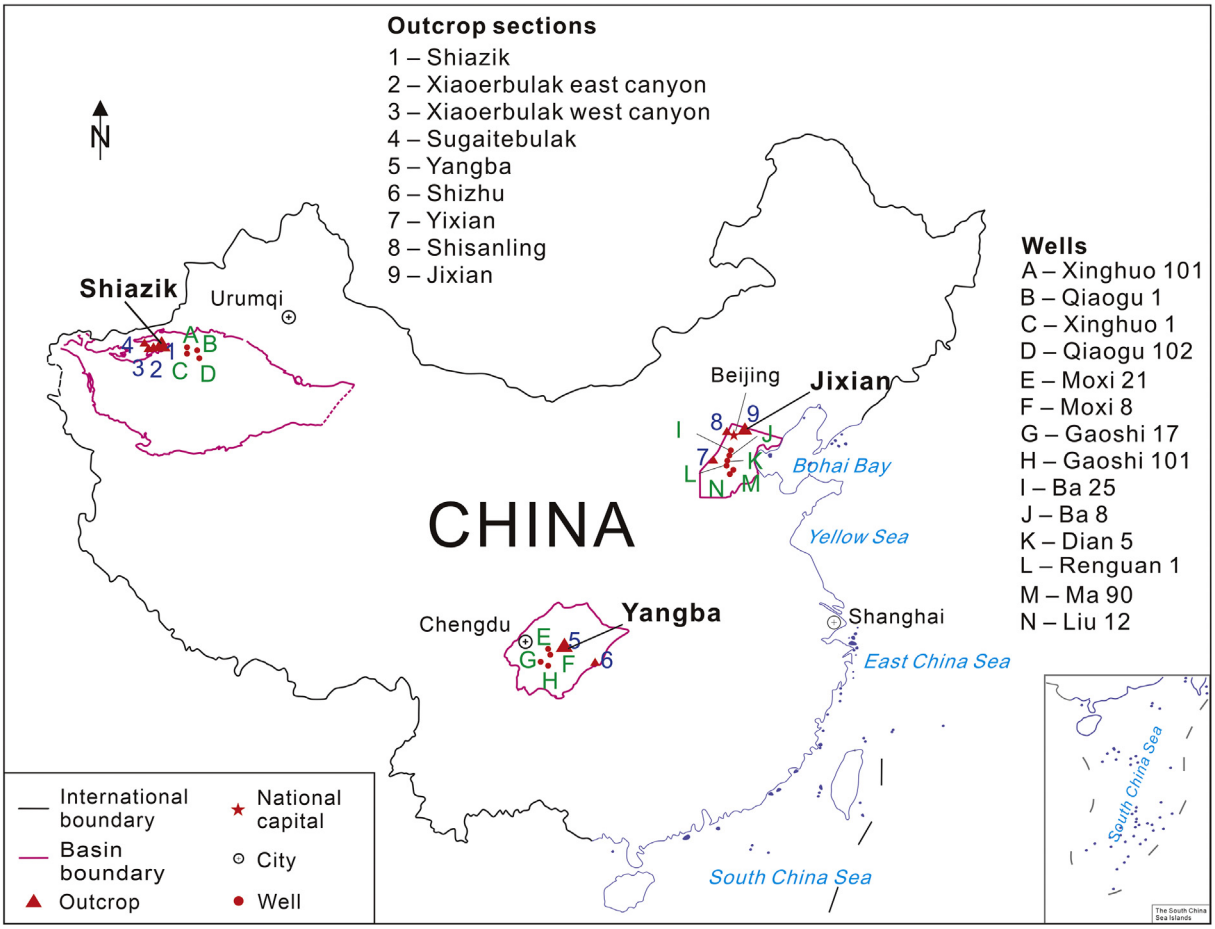

Fig. 1 Location and distribution map of the Meso-Neoproterozoic outcrops and drilling wells from typical platforms in China. The map of China is modified after the Standard Map Service of the National Administration of Surveying, Mapping and Geoinformation of China (http://bzdt.ch.mnr.gov.cn/) (No. GS(2019)1823).

Microscopically, the cabbage-shaped stromatolites contains quartz grains. In general it reflects the transgressive process from mixed tidal flat to microbial mound.

Member II of the Qigbulak Formation is 53 m thick. The lower part is composed of mound stromatolites and columnar stromatolites (1—2 m thick) with thin layers of dolomitic mudstones. The thickness of the upper stromatolites reduced to about 20 cm, and the thickness of the single layer of muddy shale is 1 m (the maximum flooding surface). The oolitic dolostone, laminar dolostone, wavy stromatolitic dolostone and algal dolostone were successively developed in the upper part. It reflects the sedimentary sequence that the microbial mound firstly transited to muddy-dolomitic flat and then evolved into grain shoal and microbial mound indicating that the relative sea level experienced a process of first rising and then falling in this period.

Member III of the Qigbulak Formation is 93.5 m thick. From the bottom upwards the lithology is dominated by algal clotting dolostone, stromatolitic dolostone and sand clastic dolostone interbedded with medium-thin bedded of mud-sized crystalline dolostone. With the thickness of grain dolostone decreasing, the thickness of dolostone increases. Thick-bedded to massive mud-sized crystalline dolostones are developed in the middle part, with the thickness of each set more than 3 m. The upper part gradually transformed into the thick massive sand clastic dolostone. At the top is a set of mud-sized to silt-sized crystalline dolostone with a thickness of about 10 m. It has an unconformable contact with the mudstone of the Cambrian Yuertusi Formation, with a weathering crust developed inbetween. In general, it reflects the sedimentary sequence of grain shoals—dolomitic flats—grain shoals, and the sea level is relatively high during the depositional period of the dolomitic flats.

2.1.2. *Yangba section of Sichuan Basin*

Compared with the Qigbulak Formation in Shiazik section, Tarim Basin, the Dengying Formation in

Table 1 Thickness of the Meso-Neoproterozoic dolostones in outcrops and drilling wells of platforms in China.

Basins	Outcrops and drilling wells	Strata unit	Thickness (m)
Tarim Basin	Xiaoerbulak west canyon section	Ediacaran Qigbulak Formation	200.80
	Shiazik section	Ediacaran Qigbulak Formation	164.50
	Sugaitebulak section	Ediacaran Qigbulak Formation	172.90
	Xiaoerbulak east canyon section	Ediacaran Qigbulak Formation	140.10
	Well Qiaogu 1	Ediacaran Qigbulak Formation	15.08
	Well Xinghuo 1	Ediacaran Qigbulak Formation	13.73
	Well Qiaogu 102	Ediacaran Qigbulak Formation	7.75
	Well Xinghuo 101	Ediacaran Qigbulak Formation	6.70
North China Basin	Jixian section	Calymmian Wumishan Formation	3416.00
	Shisanling section	Calymmian Wumishan Formation	2234.88
	Yixian section	Calymmian Wumishan Formation	1451.47
	Well Ba 8	Calymmian Wumishan Formation	1265.50
	Well Ba 25	Calymmian Wumishan Formation	1236.27
	Well Renguan 1	Calymmian Wumishan Formation	909.61
	Well Dian 5	Calymmian Wumishan Formation	769.37
	Well Liu 12	Calymmian Wumishan Formation	621.42
	Well Ma 90	Calymmian Wumishan Formation	519.05
Sichuan Basin	Yangba section	Ediacaran Dengying Formation	832.00
	Shizhu section	Ediacaran Dengying Formation	423.00
	Well Moxi 8	Ediacaran Dengying Formation	320.80
	Well Gaoshi 101	Ediacaran Dengying Formation	131.24
	Well Moxi 21	Ediacaran Dengying Formation	101.66
	Well Moxi 17	Ediacaran Dengying Formation	29.00

Yangba section, Sichuan Basin is also dominated by medium-thick bedded to massive mud-sized to silt-sized crystalline dolostone. The difference is that the microorganisms such as algae are relatively more developed in the dolostone of Yangba section (Fig. 3).

The thickness of Ediacaran Dengying Formation in Yangba section is 832 m and has an unconformable contact with the quartz sandstone layer of the underlying Guanyinya Formation. The Dengying Formation can be divided into four members.

The thickness of Member I of the Dengying Formation is 13 m. In the lower part, there is a thick layer of gray mud-sized to silt-sized crystalline dolostone, with extremely-developed vuggy fractures and pores along the lamination, and the width of vuggy fractures at the bottom is about 1 m. The upper part is mainly gray to light gray laminar stromatolitic dolostone, and the vuggy fractures and caves are relatively developed along the lamination. The sedimentary sequence of the transition from dolomitic flat to microbial mound is generally reflected.

The thickness of Member II in the Dengying Formation is 498 m and can be divided into two submembers. At the bottom part of the lower submember, there are gray medium-thick bedded to massive "grape lace-like" stromatolitic dolostone (about 30 m thick). Among which the grape lace-like structure is developed along the surface, with a diameter of 2.5—10 cm. Under the microscope, it is manifested that crystalline grains grow gradually along the vertical direction of the lace. The inner core of grape-lace is micrite component. The middle part is about 50 m, composed of the gray thick mud-sized to silt-sized crystalline dolostone with the stromatolitic dolomitic bands. The algal dolomitic bands decrease in the upper part, the mud-sized crystalline dolostone tends to have uniform density, and the fenestral structures are visible partially. The transgressive sedimentary sequence which is from microbial mound to dolomitic flat is generally reflected. In the bottom part of the upper sub-member, there are mainly gray medium-thick laminar mud-sized to silt-sized crystalline dolostone, followed by wavy stromatolitic dolostone, sand clastic dolostone and mud-sized to silt-sized crystalline dolostone with muddy bands from the bottom to top, and then develops the light gray medium-thick bedded to massive stromatolitic mud-sized crystalline dolostone with a thickness of about 30 m at the top of Member II of the Dengying Formation, with the muddy bands reducing. It reflects a transgressive—regressive cycle of the microbial mound-the dolomitic flat-microbial mound.

Member III of the Dengying Formation is a clastic layer with a thickness of 81 m. The lithologies are siltstones, muddy siltstones, and mudstones from the bottom to top. The dark mudstones at the top of the Member III indicate that the flooding surface has reached the maximum.

The thickness of Member IV in the Dengying Formation is 240 m. The lower part is mainly composed of dark

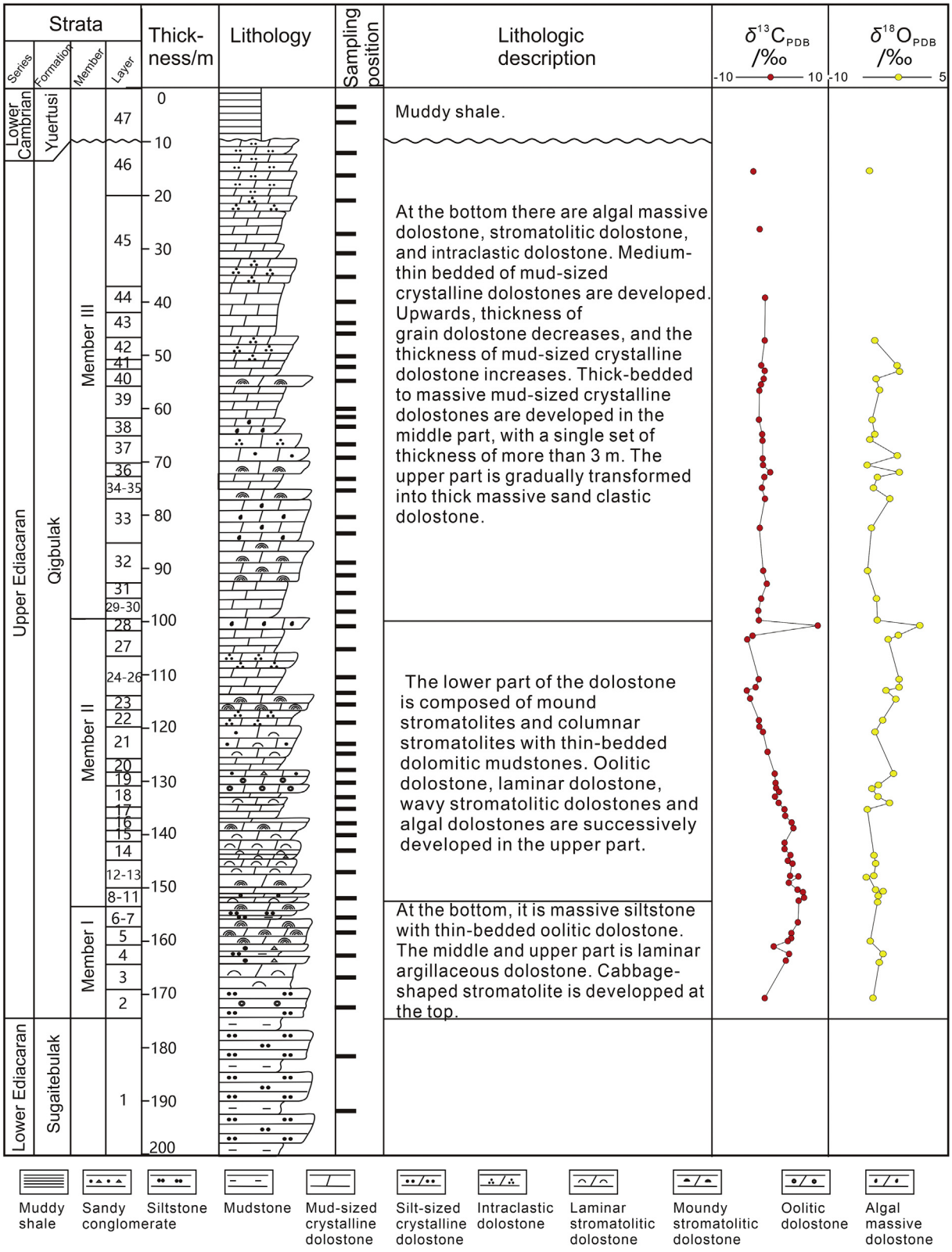

Fig. 2 Comprehensive column of the Upper Ediacaran Qigbulak Formation in Shiazik section of Tarim Basin.

gray mud-sized to silt-sized crystalline dolostone, with a small amount of gray thin-bedded dolomitic mudstones. This is a set of mud-sized to silt-sized crystalline dolostone with the maximum deposition thickness in the Yangba section, about 90 m. Compared with the Member II, there is relatively less algae and the phenomenon of

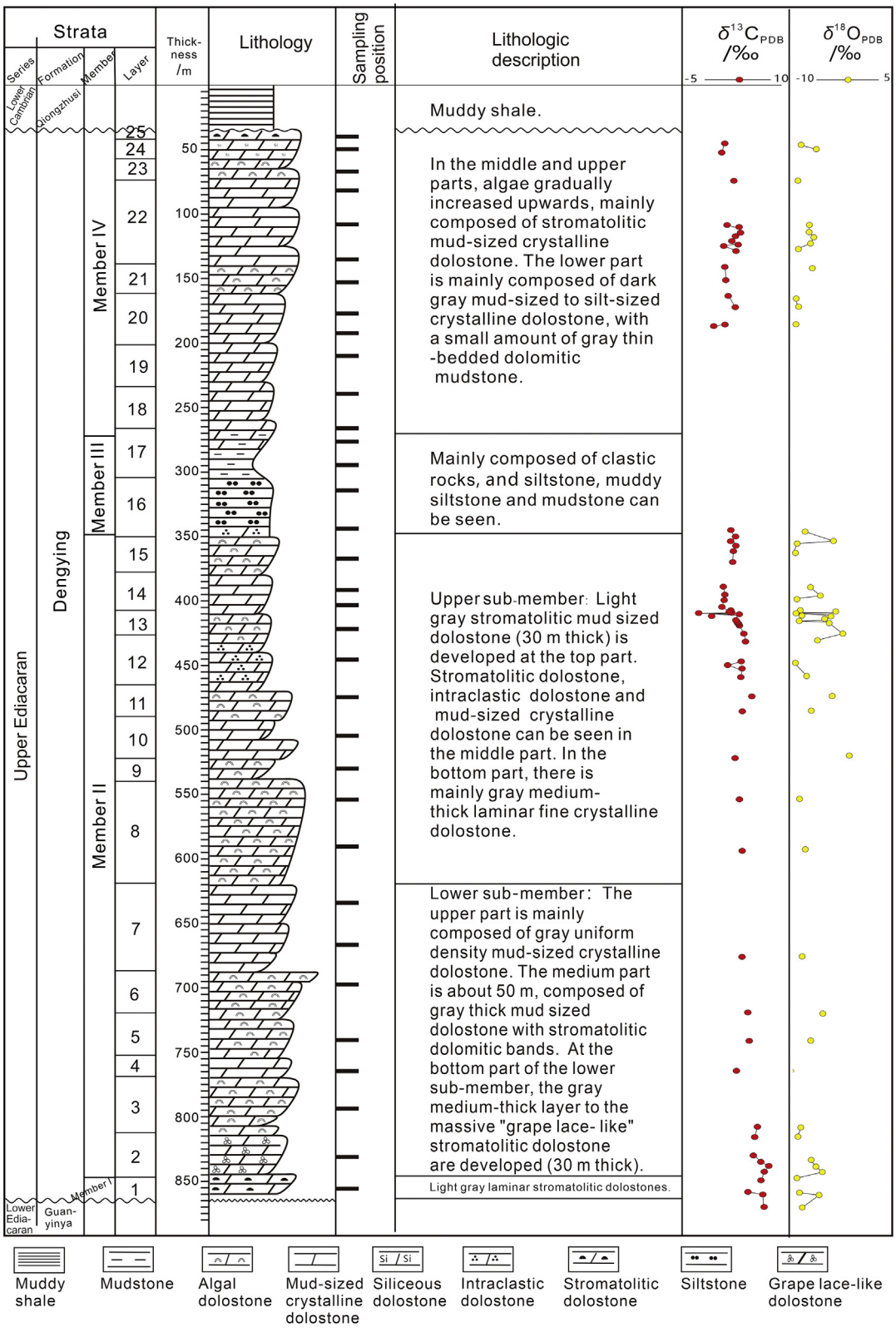

Fig. 3 Comprehensive column of the Ediacaran Dengying Formation in Yangba section of Sichuan Basin.

organic matter infiltration at the layer surface can be occasionally observed. In the middle and upper parts, algae gradually increased and stromatolitic dolostone began to appear, while the crystalline grains turned into the micrite, and then a small amount of siliceous dolostone developed upwards.

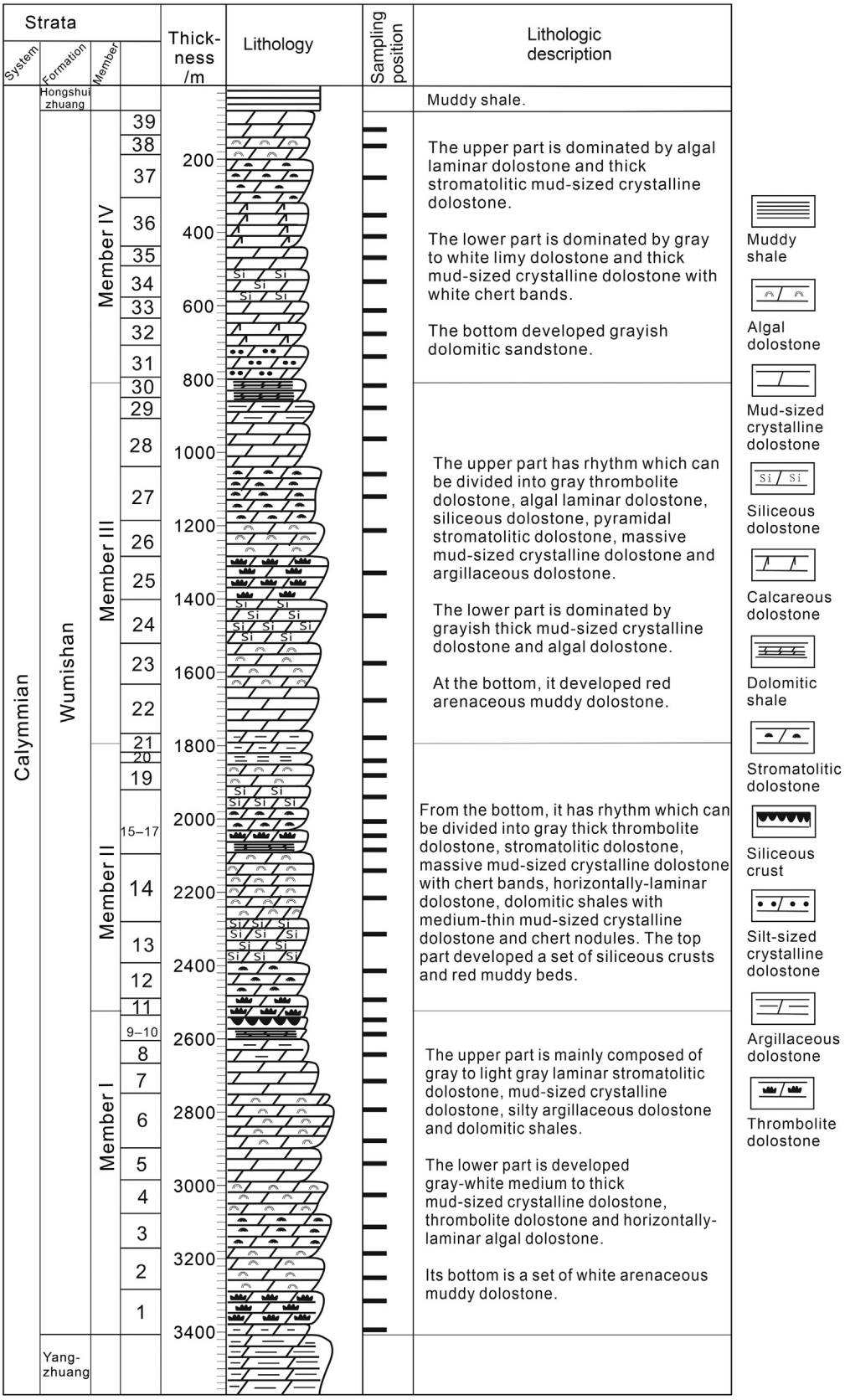

Fig. 4 Comprehensive column of the Calymmian Wumishan Formation in Jixian section of North China Basin.

Table 2 Main rock types and their distribution of the Meso-Neoproterozoic dolostone in basins of China.

Rock types		Lithology characteristics	Distribution strata
Crystalline dolostone	Mud-sized crystalline dolostone	Light gray, thin, medium-thick layer.	Widely distributed in the Meso-Neoproterozoic strata of the three studied basins.
	Silt-sized crystalline dolostone	Light gray, thin, medium-thick layer.	Less distributed in the Member I of Shiazik section, Member IV in the Dengying Section, and Member I of Wumishan Section.
	Fine-medium crystalline dolostone	Light gray, thin, medium-thick layer.	Occasionally distributed in the Member III of Shiazik section, and Member IV in the Dengying section.
Grain dolostone	Intraclastic dolostone	Light gray to gray, thin to medium layer, mostly mud-sized crystalline textures.	Mainly distributed in the Member II of Shiazik section, Member II of Dengying section.
	Oolitic dolostone	Light gray, medium layer, mostly mud-sized crystalline textures.	Occasionally distributed in the Member III of Shiazik section and Member III of Wumishan section.
	Algal sand-sized dolostone	Gray, medium layer, mostly mud-sized crystalline textures.	Mainly developed in the Member II of Shiazik section, Member II of Dengying section.
Microbial dolostone	Microbiological dolostone	Gray, medium layer, mostly mud-sized crystalline textures.	Developed in the Member II and Member III of Shiazik section, Member II of Dengying section, and Member I of Wumishan section
	Stromatolitic dolostone	Gray, medium layer, mostly mud-sized crystalline textures.	Developed in the upper layer of the Meso-Neoproterozoic strata, and more developed in Sichuan Basin than in North China Basin and Tarim Basin.

2.1.3. Jixian section of North China basin

The stratigraphic thickness of the Mesoproterozoic Calymmian Wumishan Formation in Jixian section of the North China Basin is 719—3416 m. The lithology is basically dolostone. Medium-thick bedded to massive mud-sized to silt-sized crystalline dolostone is particularly developed, which contains a large number of algal microbial textures with obvious rhythmical characteristics. It is subdivided into four lithologic members corresponding to four sedimentary semi-cycles (Fig. 4).

The Wumishan Formation in the Jixian section is 3416 m thick which conformably overlies the red argillaceous dolostone of the Yangzhuang Formation. The Wumishan Formation can be divided into four members.

Member I in the Wumishan Formation is 860 m thick. At the bottom is a set of white silty argillaceous mud-sized crystalline dolostone. The lower part of the Member I develops gray—white medium to thick mud-sized crystalline dolostone, thrombolite dolostone and horizontally-laminar algal dolostone; the upper part is mainly composed of gray to light gray laminar stromatolitic dolostone, mud-sized crystalline dolostone, silt-sized crystalline dolostone and dolomitic shales; the top is covered by a set of siliceous encrustation. The sedimentary sequence of transgression—regression in the tidal-flat environment is generally reflected.

Member II of the Wumishan Formation is 766 m thick, and shows extremely strong internal cyclicity. From the bottom to top, it can be divided into gray thick thrombolite dolostone, stromatolitic dolostone, massive mud-sized crystalline dolostone with chert bands, horizontally-laminar dolostone, dolomitic shales with medium-thin mud-sized crystalline dolostone and chert nodules, respectively. The siliceous crusts and red muddy beds are developed at the top part. Overall, it reflects a tidal-flat facies in a marine regressive environment.

Member III of the Wumishan Formation is 963 m thick. Red arenaceous dolostone is developed at the bottom; and the grayish thick mud-sized crystalline dolostone and algal dolostone dominated the lower part; the upper part is composed of a lithological rhythm which can be divided into gray thrombolite dolostone, algal laminar dolostone, siliceous dolostone, pyramidal stromatolitic dolostone, massive mud-sized crystalline dolostone, and argillaceous dolostone. Overall it reflects a sedimentary sequence of marine transgression—regression in a tidal flat environment.

Member IV of the Wumishan Formation is 827 m thick. The bottom develops grayish dolomitic sandstones. The lower part is dominated by gray—white limy dolostone and thick mud-sized crystalline dolostone with white chert bands. The upper part mainly develops algal laminar dolostone and thick stromatolitic mud-sized crystalline dolostone. Overall, it reflects a marine regression in a tidal flat environment.

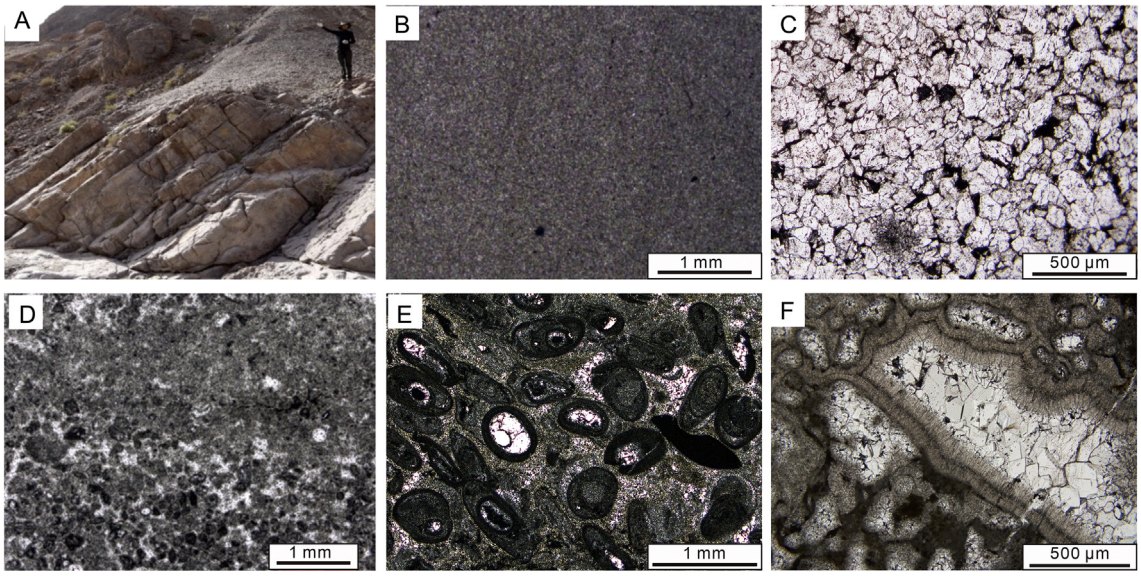

Fig. 5 The Neoproterozoic dolostones in Tarim Basin. **A)** Medium to thick mud-sized crystalline dolostone, with thickness of 22 m, 39th layer of Shiazik section, the upper part of Qigbulak Formation; the man is 1.75 m tall for scale; **B)** Mud-sized crystalline dolostone, with thickness of 6 m, 24th layer of Shiazik section, the middle part of Qigbulak Formation; **C)** Fine-medium crystalline dolostone, with thickness of 10 m, 46th layer of Shiazik section, the upper part of Qigbulak Formation, plane-polarized light; **D)** Intraclastic dolostone (the intraclasts are composed of mud-sized crystalline dolostone and have not been metasomatized), with thickness of 8 m, 42nd layer of Shiazik section, the upper part of Qigbulak Formation, cross-polarized light; **E)** Oolitic dolostone, composed of mud-sized crystalline dolostone, with thickness of 4 m, 19th layer of Shiazik section, the middle part of Qigbulak Formation, plane-polarized light; **F)** Fibrous algal dolostone, interior being filled with coarse dolostone, with thickness of 10 m, 33rd layer of Xiaoerblak section, the upper part of Qigbulak Formation, plane-polarized light.

2.2. *Classification of dolostone*

On the basis of the measurements and analyses of outcrops and drilling cores (i.e., 9 outcrops and 14 drilling cores, respectively; Fig. 1) on the Meso-Neoproterozoic strata in the basins of China, combined with the observation of 806 thin sections, we classified the dolostone into three categories (crystalline dolostone, grain dolostone, and microbial dolostone) and eight sub-categories based on the dolostone components (Table 2).

2.2.1. *Crystalline dolostone*

It mainly includes mud-sized crystalline dolostone and silt-sized crystalline dolostone (Figs. 5A, 5B, 6A, 6F, 7A, 7C), as well as a small amount of fine-mesocrystalline dolostone (Fig. 5C). Mud-sized crystalline dolostone and silt-sized crystalline dolostone are the main types of the Meso-Neoproterozoic dolostones in basins of China. From the Mesoproterozoic Wumishan Formation in North China Basin to the Neoproterozoic Qigbulak Formation in Tarim Basin and the Neoproterozoic Dengying Formation in Sichuan Basin, the color of dolostone is generally light gray to grayish white, with occasionally purple or dark gray and commonly it shows medium-thick bedded to massive textures. With dense lithology of the medium-thick bedded to massive mud-sized crystalline dolostone and by the lack of fluid channelling system necessary for diagenetic metasomatism, it shows that the dolostone is of primary sedimentary origin.

2.2.2. *Grain dolostone*

It mainly includes intraclastic dolostone (Figs. 5D, 7E), algal clotting dolostone (Fig. 5H), oolitic dolostone (Fig. 5E), fibrous algal dolostone (Fig. 5F) and algal clastic dolostone (Fig. 7D). During the entire Meso-Neoproterozoic depositional period, grain dolostone is well developed. In the Qigbulak Formation in Tarim Basin, the Dengying Formation in Sichuan Basin and the Wumishan Formation in North China Basin, the grain and matrix in the grain dolostone are mostly of mud-sized crystalline texture, indicating that these dolostones are of primary sedimentary (or penecontemporaneous) origin.

2.2.3. *Microbial dolostone*

The Meso-Neoproterozoic microbial dolostone in basins of China includes the microbial dolostone (Figs.

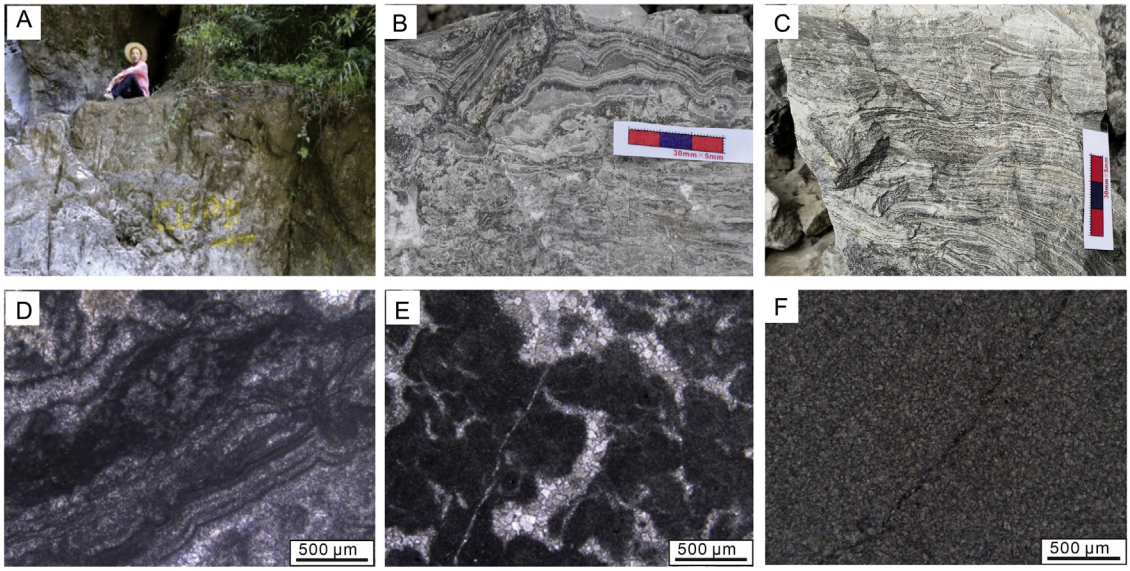

Fig. 6 The Neoproterozoic dolostones in Sichuan Basin of China. **A)** Massive mud-sized crystalline dolostone, with thickness of 24 m, Shizhu section, Member II of Dengying Formation; the man is 1.75 m tall for scale; **B)** Grape lace-like dolostone, with thickness of 4 m, Xianfeng section, Member II of the Dengying Formation; **C)** Algal laminar dolostone, Xianfeng section, Member II of the Dengying Formation; **D)** Stromatolitic dolostone (the light and dark layers of stromatolites are all composed of mud-sized crystalline dolostone; and the dark layers have a higher content of organic matters), with thickness of 16 m, 8th layer of Yangba section, the lower sub-member of Member II of Dengying Formation, plane-polarized light; **E)** Algal clotting dolostone (the algal textures are composed of mud-sized crystalline dolostone and are rich in organic matters), with thickness of 12 m, Shizhu section, the upper sub-member of Member II of Dengying Formation, plane-polarized light; **F)** Silt-sized crystalline dolostone, with thickness of 4 m, 7th layer of Yangba section, Member IV of Dengying Formation, plane-polarized light.

6B, 6C, 7B) and the stromatolitic dolostone (Figs. 6D, 7F). Stromatolitic dolostone is well developed in the Wumishan Formation in North China Basin and the Dengying Formation in Sichuan Basin, and can be identified in laminar stromatolites, wavy stromatolites and columnar stromatolites formed in the intertidal to

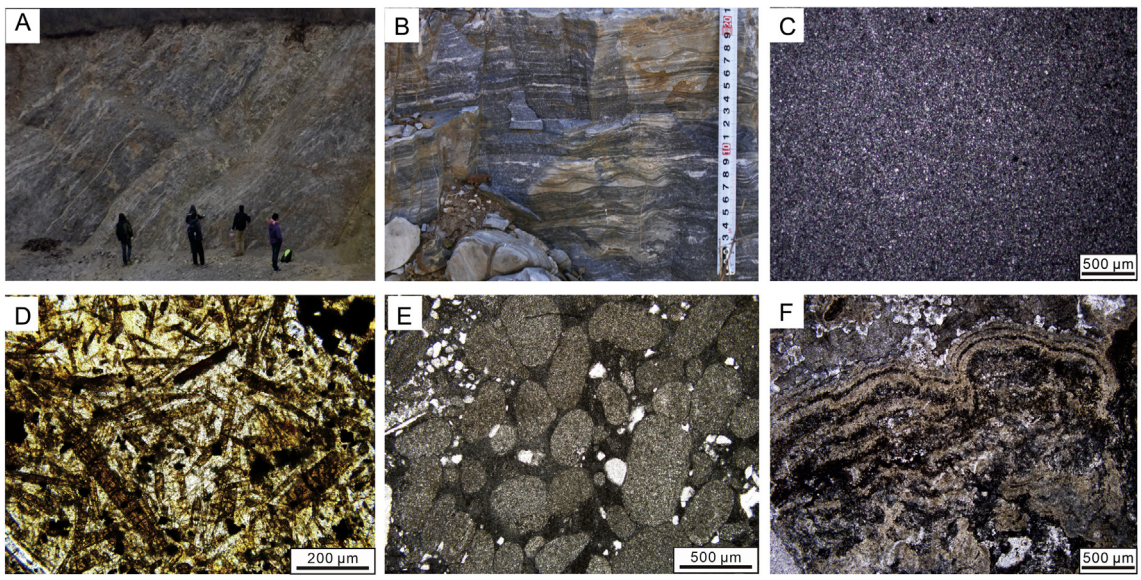

Fig. 7 The Mesoproterozoic dolostones in North China Basin of China. **A)** Massive mud-sized crystalline dolostone, with thickness of 146 m, 22nd layer of Jixian section, Member III of Wumishan Formation; **B)** Algal laminar dolostone, with thickness of 14 m, Member II of Yixian section, Wumishan Formation; **C)** Silt-sized crystalline dolostone, with thickness of 45 m, 31st layer of Jixian section, Wumishan Formation, plane-polarized light; **D)** Algal clastic dolostone, with thickness of 35 m, 19th layer of Jixian section, Wumishan Formation, plane-polarized light; **E)** Intraclastic dolostone, with thickness of 58 m, 26th layer of Jixian section, Wumishan Formation, plane-polarized light; **F)** Stromatolitic dolostone, with thickness of 112 m, 27th layer of Jixian section, Wumishan Formation, plane-polarized light.

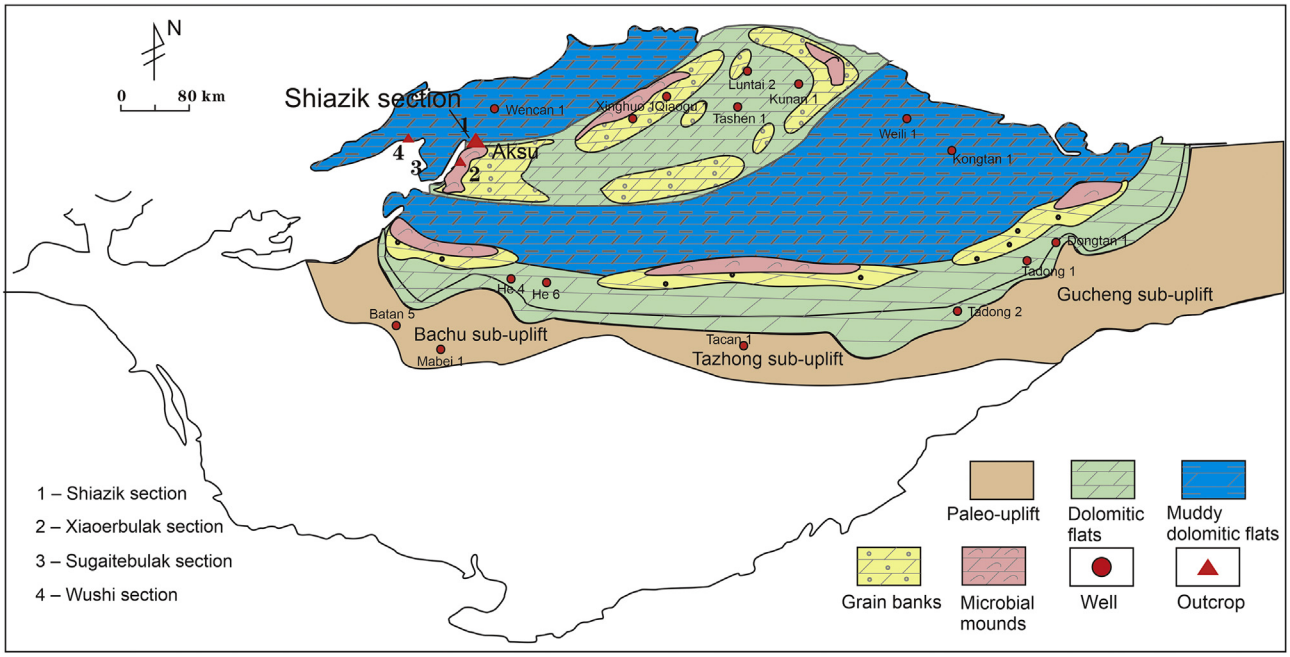

Fig. 8 Lithofacies palaeogeographic map during the depositional period of Member III of the Qigbulake Formation in Tarim Basin. Mud-sized to silt-sized crystalline dolostones were widely distributed in the whole Tarim basin during this period, microbial dolostone and grain dolostone that were composed of mud-sized to silt-sized crystallines were deposited in high palaeogeomorphologic areas, and the normally mud-sized to silt-sized crystalline dolostones were deposited in open or restricted platform areas.

subtidal zone. In the three basins, the microbial dolostone is mainly mud-sized crystalline textures with distinctly primary sedimentary characteristics.

Indicated by outcrop and core observation, and the microscopic analysis, the proportion of mud-sized crystalline dolostone (or silt-sized crystalline dolostone) of Ediacaran Qigbulak Formation in the Xiaoerbulak section, the Shiazik section and the Well Qiaogu 8 in Tarim Basin ranges between 93% and 97%. The proportion of mud-sized crystalline dolostone (or silt-sized crystalline dolostone) of Ediacaran Dengying Formation in the Yangba section, the Shizhu section and the Well Moxi 8 in Sichuan Basin ranges between 87% and 91%. The proportion of mud-sized crystalline dolostone (or silt-sized crystalline dolostone) of the Wumishan Formation in the Jixian section and the Well Ba 8 in North China Basin ranges between 86% and 95%.

3. Sedimentary palaeogeography during the Meso-Neoproterozoic depositional period

Based on the measurement of 23 sections (outcrops and drilling cores) in the three basins (Fig. 1), and combined with the regional geological information (Hebei Bureau of Geology and Mineral Resources Exploration, 1982; Sichuan Bureau of Geology and Mineral Resources, 1989; Xinjiang Bureau of Geo-Exploration and Mineral Development, 1993) and previous research results of our team, it is considered that in the basins such as Tarim Basin, North China Basin, and Sichuan Basin, the sediments deposited mainly in the environments from tidal flat to platform during the Meso-Neoproterozoic period.

The reconstruction results of paleogeomorphology show that the central part of the basement was an uplift in the east—west direction, and the north and south sides were relatively flat platforms before the depositional period of Neoproterozoic Qigbulak Formation in Tarim Basin. During the sedimentary period of Qigbulak Formation, there were grain shoals and microbial mounds formed on the middle uplift, and the deposition of dolomitic flats and mixed tidal flats were formed in the platform areas on both sides (Fig. 8).

During the depositional period of Mesoproterozoic Wumishan Formation, a wide range of tidal flats were developed in the North China Basin, and supratidal, intertidal and subtidal zones were successively developed from south to north (Fig. 9).

Various sedimentary facies, which were mainly developed in platform and inter-platform environment are found in the Neoproterozoic Dengying Formation in Sichuan Basin (Wang, 2017). The geophysical data show that syngenetic faults also developed in this period and continuous rifting formed the sedimentary

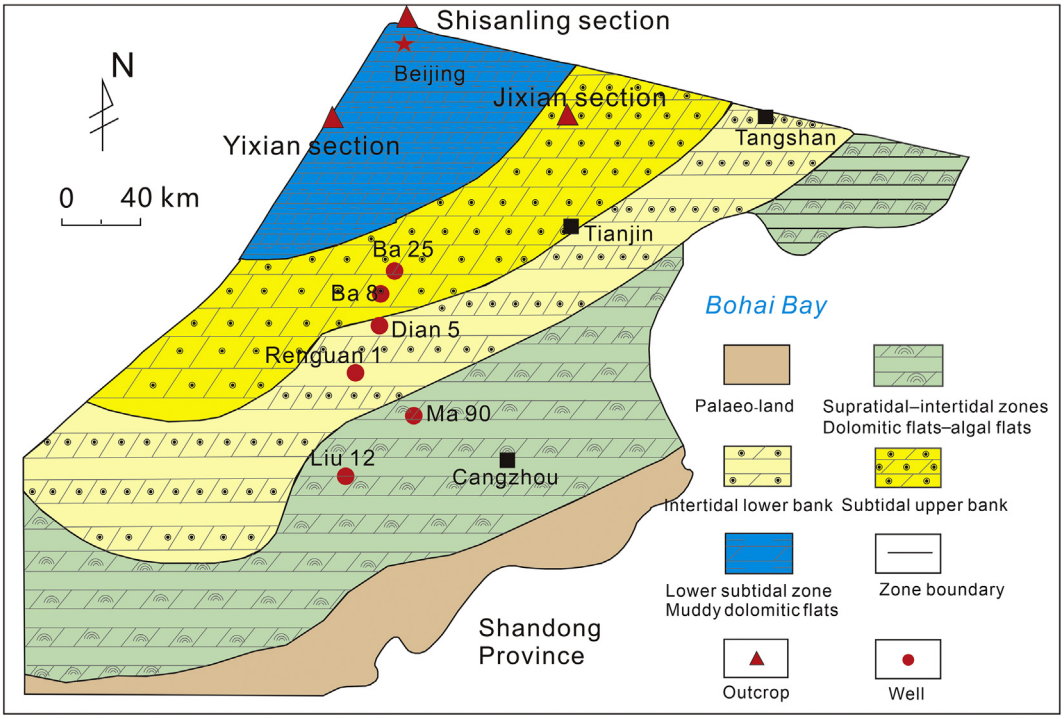

Fig. 9 Lithofacies palaeogeographic map during the depositional period of Wumishan Formation in Beijing—Tianjin—Hebei region, North China. The mud-sized to silt-sized crystalline dolostones spread all over the North China Platform. The argillaceous dolostone mainly distributes in lower subtidal zone, and the grain mud-sized crystalline dolostone is in lower intertidal to upper subtidal zone; additionally, the algal mud-sized crystalline dolostone develops in the intertidal to supratidal zone.

palaeogeographic framework of platforms alternates with basins (Fig. 10).

In these platforms, the main deposits of dolomitic flats are mud-sized crystalline dolostone, microbial mud-sized crystalline dolostone, and a small amount of mud-sized to silt-sized crystalline dolostone, such as Ediacaran dolomitic flats in Tarim Basin, dolomicritic flats and algae dolomitic flats of the Wumishan Formation in central part of North China Basin. The grain shoals are mainly distributed in high geomorphologic area of the sedimentary basement in the platform, and the lithologies are mainly composed of grain dolostone, including sand clastic dolostone, oolitic dolostone, and algal dolostone, reflecting shallow water sedimentary environment with strong hydrodynamic condition. The microbial mounds are generally distributed on the tidal flats or the grain shoals in the platform, and the lithologies are mainly stromatolitic dolostones, including laminar dolostone, wavy stromatolitic dolostone and columnar (cabbage-shape) stromatolitic dolostone, reflecting the sedimentary environment of tidal or platform interior shoal.

From the Mesoproterozoic Wumishan depositional period in the central North China Basin to the Late Neoproterozoic period in Tarim Basin and Sichuan Basin, there were generally tidal flat and carbonate platform environments controlled by the "uplift-sag" structure, and crystalline dolostone, grain dolostone and microbial dolostone were well developed. It is worth noting that these dolostones are generally of mud-sized crystalline textures, indicating the sedimentary components of microbial mounds in the northern uplift of Tarim Basin, tidal flat in the central North China Basin and oolitic shoals in the limited platform of Sichuan Basin. Lithologies were basically mud-sized crystalline dolostone, including sand clastic dolostone and oolites dolostone in the Meso-Neoproterozoic, no matter how strong or weak the hydrodynamic conditions were.

4. Geochemical index

4.1. Homogeneity of oxygen-carbon isotopes in dolostones with different textures

Stable isotope analysis such as $\delta^{13}C$ and $\delta^{18}O$ can be used to reconstruct the liquid properties of dolostone precipitation, especially the value of $\delta^{13}C$, which is little affected by post-sedimentary diagenesis (Keith and Weber, 1964; Taylor, 1974; Anderson and Arthor,

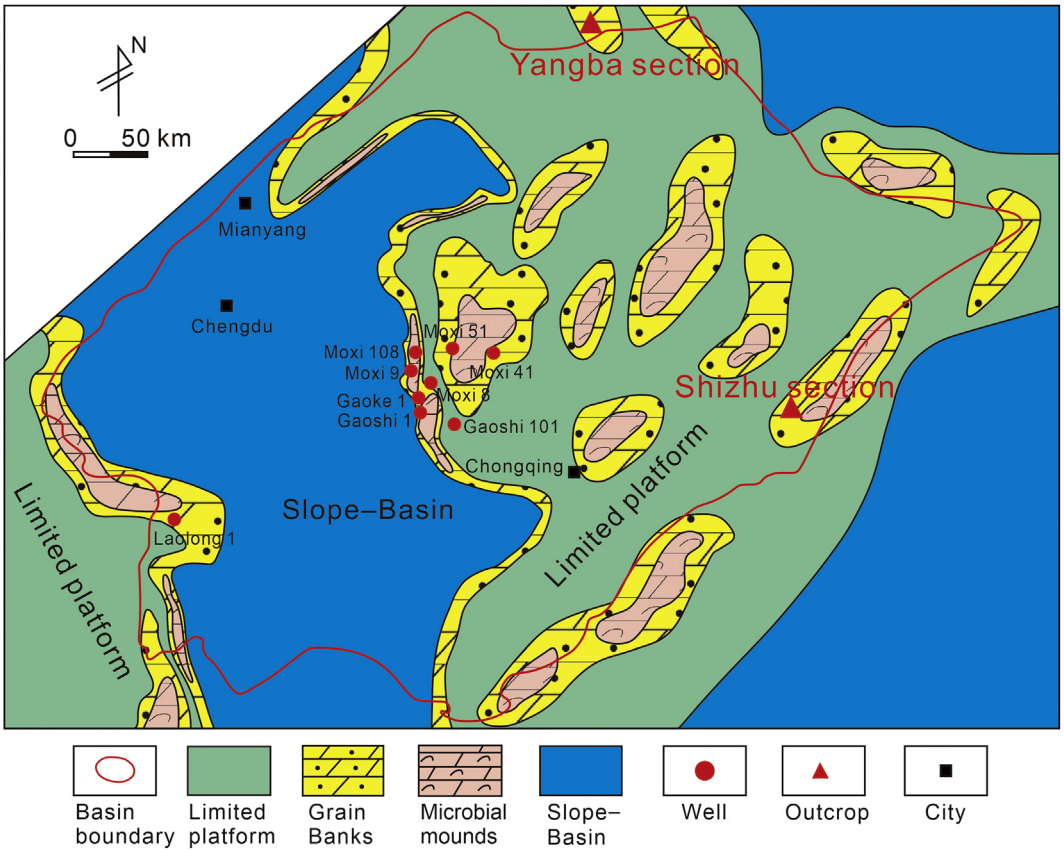

Fig. 10 Lithofacies palaeogeographic map during the depositional period of Member IV of Dengying Formation in Sichuan Basin (modified from Wang, 2017). Mud-sized to silt-sized crystalline dolostones were widely developed in the carbonate platform area on both sides of the deep faults. Grain dolostone and microbial dolostone with dolomicrite as the main component were developed on the platform margin or in the area of high geomorphology within the platforms.

1983; Veizer *et al.*, 1999; Qian *et al.*, 2012; Husson *et al.*, 2015; Ren *et al.*, 2016). In this study, dolostone samples of Dengying Formation from Yangba section in Sichuan Basin were sent to the Institute of Geology and Geophysics, Chinese Academy of Sciences for carbon and oxygen isotope analysis according to sedimentary structure (stromatolithic structure, thrombolite structure, and massive structure) and grain size (mud-sized, silt-sized, and fine-grain). Based on this, the zoning characteristics of dolostone with different sedimentary components and structures are discussed. The results show that there is no obvious difference in the carbon and oxygen isotopes distribution of dolostone with different sedimentary structures or grain sizes. The main distributed mud-sized crystalline dolostone and silt-sized crystalline dolostone or rare fine crystalline dolostone have a basically similar carbon and oxygen isotope distribution characteristic (Table 3; Fig. 11), indicating that there is no obvious difference in genesis among different types of dolostone of Dengying Formation in this area, or that they have the same genetic mechanism.

4.2. *Geochemical reflection of the depositional temperature*

The carbon and oxygen isotopes analysis results of 96 samples from Shiazik section of Tarim Basin and Yangba section of Sichuan Basin show that the carbon isotopes distribution of each sample is highly similar to the global carbon isotopes change trend of carbonates in the same period (Fig. 12). Carbon isotopes can reflect the characteristics of seawater during the sedimentary period, and they are less affected by diagenesis after carbonates deposition (Epstein *et al.*, 1953). This indicates that the characteristics of seawater during the deposition of Qigbulak Formation in Tarim Basin and the Dengying Formation of Sichuan Basin are highly consistent with the characteristics of seawater media reflected by the global

Table 3 Carbon and oxygen isotopes of dolostone with different sedimentary structures or crystal textures of Dengying Formation in Sichuan Basin and Qigbulak Formation in Tarim Basin.

Sample	Outcrop	Depth (m)	δ^{18}OPDB (‰)	δ^{13}CPDB (‰)	Crystal texture	Sedimentary structure
YB-D-239	Yangba	35.10	−7.6	0.6	Silt-sized crystalline	Massive
YB-D-233	Yangba	48.57	−9.0	0.2	Silt-sized crystalline	Stromatolithic
YB-D-232	Yangba	51.20	−6.4	0.0	Silt-sized crystalline	Stromatolithic
YB-D-219	Yangba	74.34	−9.2	1.4	Silt-sized crystalline	Stromatolithic
YB-D-202	Yangba	109.50	−11.6	0.7	Mud-sized crystalline	Massive
YB-D-201	Yangba	111.48	−7.5	2.5	Mud-sized crystalline	Massive
YB-D-200	Yangba	116.08	−7.5	2.7	Mud-sized crystalline	Massive
YB-D-199	Yangba	119.36	−6.8	1.9	Silt-sized crystalline	Massive
YB-D-198	Yangba	120.68	−11.1	1.7	Silt-sized crystalline	Massive
YB-D-196	Yangba	123.31	−7.3	1.9	Silt-sized crystalline	Massive
YB-D-195	Yangba	124.95	−12.7	0.2	Silt-sized crystalline	Massive
YB-D-194	Yangba	128.89	−9.4	1.7	Silt-sized crystalline	Massive
YB-D-191	Yangba	144.01	−7.1	0.4	Silt-sized crystalline	Stromatolithic
YB-D-189	Yangba	150.91	−10.3	0.5	Silt-sized crystalline	Massive
YB-D-186	Yangba	166.03	−9.7	1.1	Silt-sized crystalline	Thrombolite
YB-D-184	Yangba	170.30	−9.3	1.7	Silt-sized crystalline	Massive
YB-D-177	Yangba	185.09	−9.6	0.1	Silt-sized crystalline	Massive
YB-D-176	Yangba	186.08	−11.7	−0.8	Silt-sized crystalline	Massive
YB-D-165	Yangba	346.46	−8.1	1.4	Silt-sized crystalline	Stromatolithic
YB-D-164	Yangba	351.06	−10.1	1.8	Silt-sized crystalline	Stromatolithic
YB-D-163	Yangba	352.38	−3.8	1.5	Silt-sized crystalline	Stromatolithic
YB-D-162	Yangba	355.01	−9.3	2.0	Silt-sized crystalline	Stromatolithic
YB-D-161	Yangba	363.55	−9.8	1.6	Silt-sized crystalline	Stromatolithic
YB-D-160	Yangba	368.81	−10.2	1.5	Silt-sized crystalline	Thrombolite
YB-D-154	Yangba	392.14	−7.0	0.2	Mud-sized crystalline	Stromatolithic
YB-D-153	Yangba	395.43	−5.8	0.4	Mud-sized crystalline	Stromatolithic
YB-D-151	Yangba	398.06	5.1	1.0	Mud-sized crystalline	Massive
YB-D-148	Yangba	403.32	−10.6	−0.1	Mud-sized crystalline	Massive
YB-D-145-8	Yangba	407.00	−9.1	1.4	Mud-sized crystalline	Stromatolithic
YB-D-145-6	Yangba	407.50	2.7	1.7	Mud-sized crystalline	Massive
YB-D-145-4	Yangba	407.92	−9.2	1.6	Mud-sized crystalline	Thrombolite
YB-D-145-2	Yangba	407.00	0.1	1.1	Mud-sized crystalline	Thrombolite
YB-D-144	Yangba	409.56	−4.2	2.2	Mud-sized crystalline	Massive
YB-D-142-a	Yangba	415.00	−4.9	2.0	Mud-sized crystalline	Stromatolithic
YB-D-142-b	Yangba	414.16	−9.0	2.2	Mud-sized crystalline	Stromatolithic
YB-D-142-c	Yangba	413.00	−4.7	2.2	Mud-sized crystalline	Stromatolithic
YB-D-141-a	Yangba	417.00	−10.7	2.2	Mud-sized crystalline	Massive
YB-D-141-b	Yangba	415.81	−10.2	2.4	Mud-sized crystalline	Stromatolithic
YB-D-137	Yangba	424.35	−2.4	3.2	Mud-sized crystalline	Massive
YB-D-136	Yangba	430.92	−5.9	3.4	Mud-sized crystalline	Stromatolithic
YB-D-132	Yangba	439.14	−8.8	3.1	Mud-sized crystalline	Massive
YB-D-117	Yangba	483.18	−7.0	3.0	Silt-sized crystalline	Stromatolithic
YB-D-106	Yangba	522.62	−1.6	2.0	Mud-sized crystalline	Thrombolite
YB-D-98	Yangba	551.87	−9.3	2.5	Mud-sized crystalline	Thrombolite
YB-D-86	Yangba	591.96	−8.2	2.9	Silt-sized crystalline	Thrombolite
YB-D-71	Yangba	676.75	−8.7	3.2	Mud-sized crystalline	Stromatolithic
YB-D-60	Yangba	719.48	−5.5	3.8	Silt-sized crystalline	Massive
YB-D-54	Yangba	737.55	−7.3	4.1	Silt-sized crystalline	Thrombolite
YB-D-47	Yangba	762.20	−10.0	2.0	Silt-sized crystalline	Stromatolithic
YB-D-26	Yangba	805.58	−8.9	5.1	Silt-sized crystalline	Thrombolite
YB-D-24	Yangba	811.50	−9.1	4.9	Mud-sized crystalline	Thrombolite
YB-D-19	Yangba	827.93	−11.5	5.0	Silt-sized crystalline	Thrombolite
YB-D-17	Yangba	831.22	−7.0	5.7	Fine crystalline	Thrombolite
YB-D-16	Yangba	832.86	3.4	6.0	Fine crystalline	Thrombolite
YB-D-15	Yangba	834.18	−6.5	6.9	Fine crystalline	Massive
YB-D-13	Yangba	839.76	−5.5	6.2	Fine crystalline	Stromatolithic
YB-D-11	Yangba	844.04	−9.5	5.9	Fine crystalline	Massive
YB-D-6	Yangba	854.22	−8.6	4.3	Fine crystalline	Massive
YB-D-5	Yangba	856.85	−6.0	6.0	Silt-sized crystalline	Thrombolite
YB-D-1	Yangba	864.74	−8.3	6.1	Silt-sized crystalline	Massive

Table 3 — (*continued*)

Sample	Outcrop	Depth (m)	δ^{18}OPDB (‰)	δ^{13}CPDB (‰)	Crystal texture	Sedimentary structure
Sq-24	Shiazik	32.51	1.5	−5.0	Mud-sized crystalline	Massive
Sq-25-2	Shiazik	35.62	1.1	−6.6	Mud-sized crystalline	Massive
Sq-26-1	Shiazik	39.65	2.1	−4.4	Mud-sized crystalline	Massive
Sq-26-2	Shiazik	41.25	2.4	−4.4	Mud-sized crystalline	Massive
Sq-27-2	Shiazik	46.37	1.2	−6.3	Silt-sized crystalline	Massive
Sq-28-1	Shiazik	51.36	1.6	−4.7	Mud-sized crystalline	Stromatolithic
Sq-29-2	Shiazik	67.32	9.0	−0.7	Mud-sized crystalline	Massive
Sq-30-2	Shiazik	69.54	2.4	−10.4	Mud-sized crystalline	Thrombolite
Sq-31-2	Shiazik	74.34	2.7	−8.3	Mud-sized crystalline	Thrombolite
Sq-32-1	Shiazik	79.38	3.3	−11.6	Mud-sized crystalline	Stromatolithic
Sq-32-2	Shiazik	83.68	2.9	−9.9	Mud-sized crystalline	Thrombolite
Sq-33-2	Shiazik	95.38	2.5	−9.2	Mud-sized crystalline	Thrombolite
Sq-34-2	Shiazik	102.34	3.1	−6.0	Mud-sized crystalline	Thrombolite
Sq-35-2	Shiazik	112.37	2.8	−8.9	Mud-sized crystalline	Thrombolite
Sq-36-2	Shiazik	119.54	3.1	−8.2	Silt-sized crystalline	Stromatolithic

paleo-seawater carbon isotopes during the same period (Wood *et al.*, 2019).

Oxygen isotopes can be used to estimate the temperature of the ancient seawater (Epstein *et al.*, 1951; Keith and Weber, 1964; Shackleton, 1974; Erez and Luz, 1983; Wei *et al.*, 2006; Ren *et al.*, 2016). According to the oxygen isotope analysis of the Qigbulak Formation dolostone in the Shiazik section of Tarim Basin and the dolostone of the Dengying Formation in Yangba section of Sichuan Basin, the isotopic temperature of the Neoproterozoic seawater in basins in China was relatively high. For example, the seawater temperature was 15.38—48.2 °C (average 30.1 °C) during the depositional period of Qigbulak Formation in Tarim Basin, and was 16—47.55 °C (average 31.86 °C) during that of Dengying Formation in Sichuan Basin.

5. Preliminary results and discussion

5.1. *Essential characteristics of primary dolostone*

The analysis results of petrology, sedimentary environment, and geochemistry indicate that there are large-scale and widely distributed primary dolostones in the Meso-Neoproterozoic in platforms of China, including the Upper Ediacaran Qigbulak Formation of the Neoproterozoic in Tarim Basin, the Upper Ediacaran Dengying Formation of the Neoproterozoic in Sichuan Basin and the Calymmian Wumishan Formation of the Mesoproterozoic in North China Basin, which have primary dolomite characteristics.

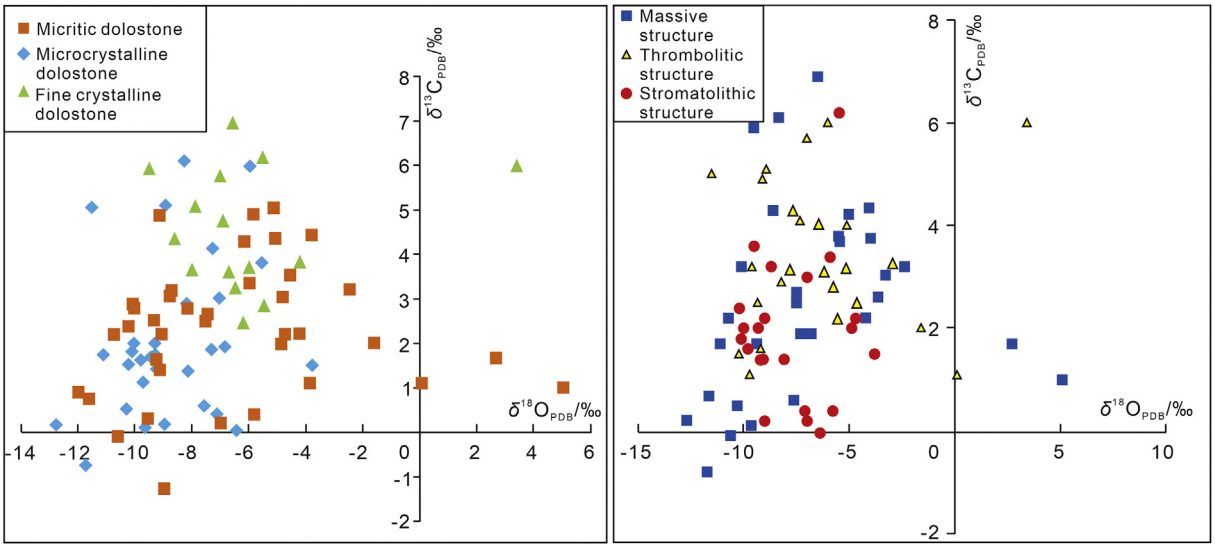

Fig. 11 Cross-plot of carbon and oxygen isotopes of dolostones with different sedimentary structures and crystal textures of Dengying Formation in Sichuan Basin and Qigbulak Formation in Tarim Basin.

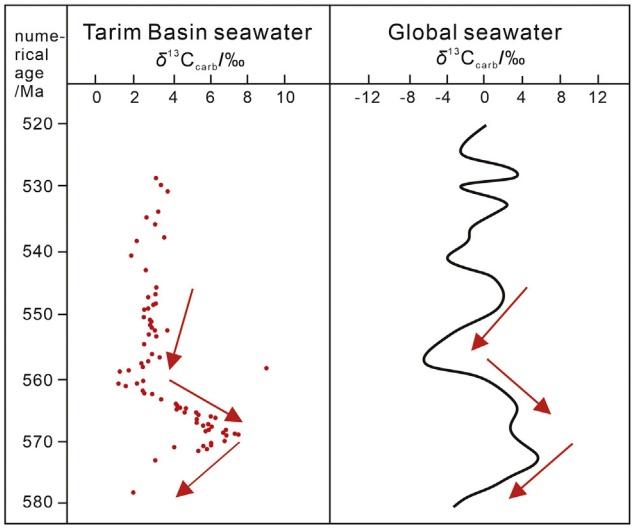

Fig. 12 Variation trend of carbon isotope from dolostone of the Qigbulak Formation in Shiazik section, Tarim Basin and a comparison with global changing curve.

5.1.1. Petrological characteristics

The crystal sizes and shapes of dolostone reflect the nucleation and growth dynamics of dolostone. The primary dolostones are formed by precipitation of a large number of mineral crystals during the deposition period, and have a very fine mud-sized crystalline form. From outcrops to drilling cores, the three Meso-Neoproterozoic cratonic basins, i.e., Tarim Basin, North China Basin, and Sichuan Basin, respectively, abnormally developed thick-bedded to massive mud-sized crystalline dolostone, with a thickness accounting for 86%—97% of the total strata. The secondary metasomatism of these massive mud-sized crystalline dolostones and a small amount of silt-sized crystalline dolostones, whether they contain the microorganisms such as algae and fungi or not, is not developed, indicating that these Meso-Neoproterozoic dolostones dominated by mud-sized crystalline dolostones are formed by primary precipitation.

5.1.2. Sedimentary palaeogeographic characteristics

Unlike the distribution of dolostone since the Phanerozoic, the penecontemporaneous mud-sized crystalline dolostones are mainly developed in the oxidation and salinization environment of supratidal and intertidal zones, or salinized lagoon in subtidal zone, and the penecontemporaneous dolostone with fine grains to medium coarse grains are mainly distributed in the platform environments outside the subtidal zone. On the other hand, the Meso-Neoproterozoic mud-sized crystalline dolostones cover almost all the sea basins at that time and are developed abnormally widely in the open or restricted platform environments besides the supratidal zone, intertidal zone, and subtidal zone. The sub-types of these primary mud-sized crystalline dolostones are controlled by the “uplift-sag” pattern of the paleo-basement on the plane, which means that the mud-sized crystalline dolostones are mainly developed in the lower parts, while the granular mud-sized crystalline dolostones or moundy stromatolitic mud-sized crystalline dolostones are developed in the upper parts.

5.1.3. Geochemical characteristics

There is no obvious difference in the division of carbon and oxygen isotope ratios between dolostones with different crystalline textures (i.e., mud-sized crystalline dolostone, and a small amount of silt-sized and fine-sized crystalline dolostone), and with different sedimentary structures (i.e., thin bedded, medium-thick bedded, and massive dolostone), which is consistent with the global seawater background values in the same geohistorical period, indicating that the structural coarsening of these small amounts of silt-sized and fine-sized crystalline dolostones are caused by self-generating and enhancing of mud-sized crystalline dolostones, rather than by secondary metasomatism. It means that similar as the mud-sized crystalline dolostones, both silt-sized and fine-sized crystalline dolostones are of primary precipitation origin.

5.2. Discussion

In view of the widespread and abnormal development of massive dolostone deposited in the Meso-Neoproterozoic, the first scientific problem involved is the source of the massive amount of Mg^{2+}, and the second is the sedimentary dynamic mechanism of the primary precipitation of massive dolostone. These two issues are both independent and interrelated.

5.2.1. Was the massive Mg^{2+} from the deep crust (mantle)?

Most of the dolostones in the Phanerozoic strata are penecontemporaneous dolostone of epigenetic metasomatism. An important reason for the non-primary origin is whether the concentration of Mg^{2+}

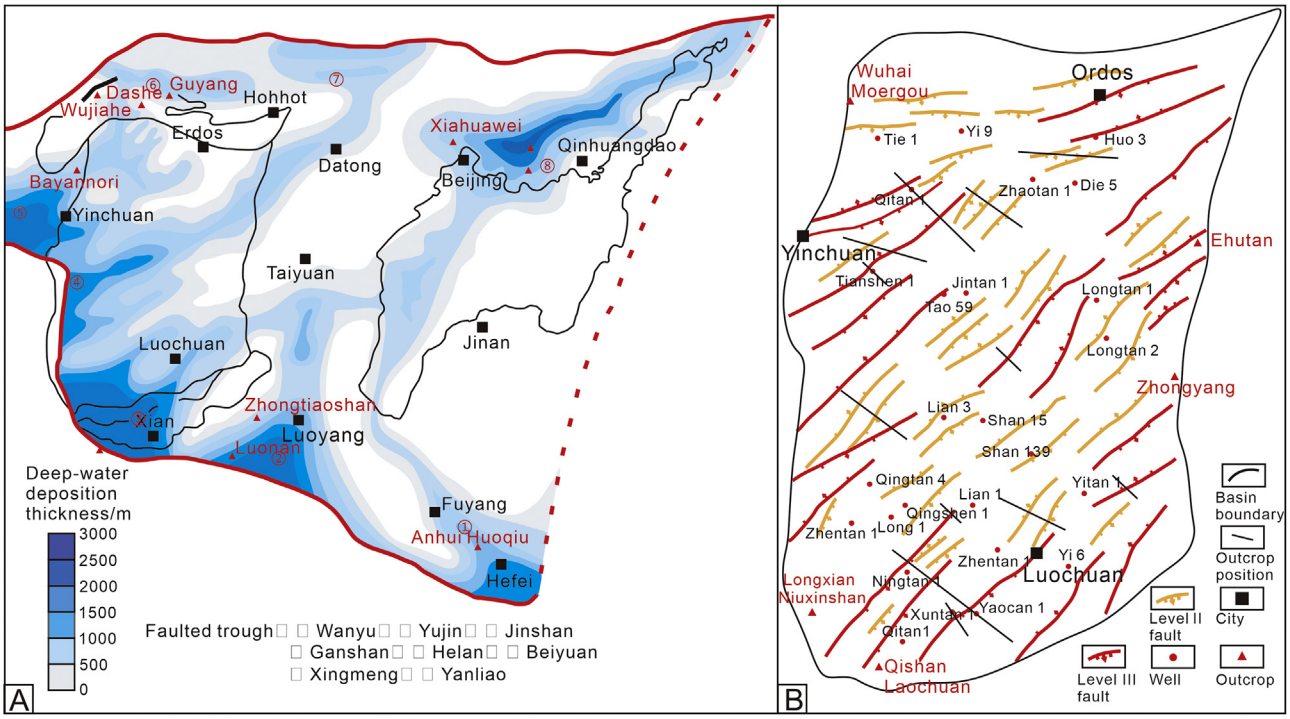

Fig. 13 Distribution of main aulacogens in North China (**A**) and synsedimentary faults in Ordos, western North China (**B**) during the Meso-Neoproterozoic (modified from Du *et al.*, 2019; Wei *et al.*, 2019).

in seawater since the Phanerozoic is not as high as that in the Proterozoic (de Dolomieu, 1791; von der Borch, 1976; Botz and von der Borch, 1984). Evidence from the composition of primary fluid inclusions in marine halite suggests that (Horita *et al.*, 2002; Timofeeff *et al.*, 2006), during the geological period, the concentration of Mg^{2+} in seawater fluctuated periodically, and the Meso-Neoproterozoic seawater shows the characteristics of being rich in Mg^{2+}. The concentration of Mg^{2+} exceeded 67 mol/kg, which could be much higher than that in most of the Phanerozoic geological stages.

The following question is whether the high concentration of Mg^{2+} in seawater of the platforms of the Proterozoic came from the deep crust (mantle). Related studies showed that the syngenetic rifts' activities were very frequent and the deep faults were widely developed during the Meso-Neoproterozoic period in North China Basin and Tarim Basin due to the impact of cracking of supercontinent such as Rodinia (White, 1981; Jiang *et al.*, 2017; Wu *et al.*, 2017; Du *et al.*, 2019; Wei *et al.*, 2019) (Fig. 13). Similarly, the Neoproterozoic syngenetic deep faults in Sichuan Basin were also abnormally developed and gradually decreased from Neoproterozoic to Early Paleozoic (Fig. 14). These extremely active and widely developed deep faults may provide channels for the upward migration of deep Mg^{2+} and other materials.

5.2.2. *Whether the sedimentary dynamics of the primary dolostone were triggered by high temperature and some awaiting-unveiled catalysts such as Fe^{2+}*

In addition to the high concentration of Mg^{2+} in seawater, whether the mass deposition of Meso-Neoproterozoic primary dolostone was controlled by other sedimentary chemical kinetic factors such as high seawater temperature?

Previous studies have shown that there are many kinetic factors affecting the primary dolomitic deposition, such as the metabolism of algae and other microorganisms, which may produce catalysts for the chemical deposition of dolostone. However, the microorganisms were not well developed during the Early Meso-Neoproterozoic, especially in the open platform with deep water. Therefore, the life activities of microorganisms are unlikely to be the main factors promoting the deposition of these widely distributed thick to massive primary dolostone (Vasconcelos *et al.*, 1995; Turner, 2009).

Therefore, the high-temperature atmospheric conditions caused by the concentration of CO_2 in the

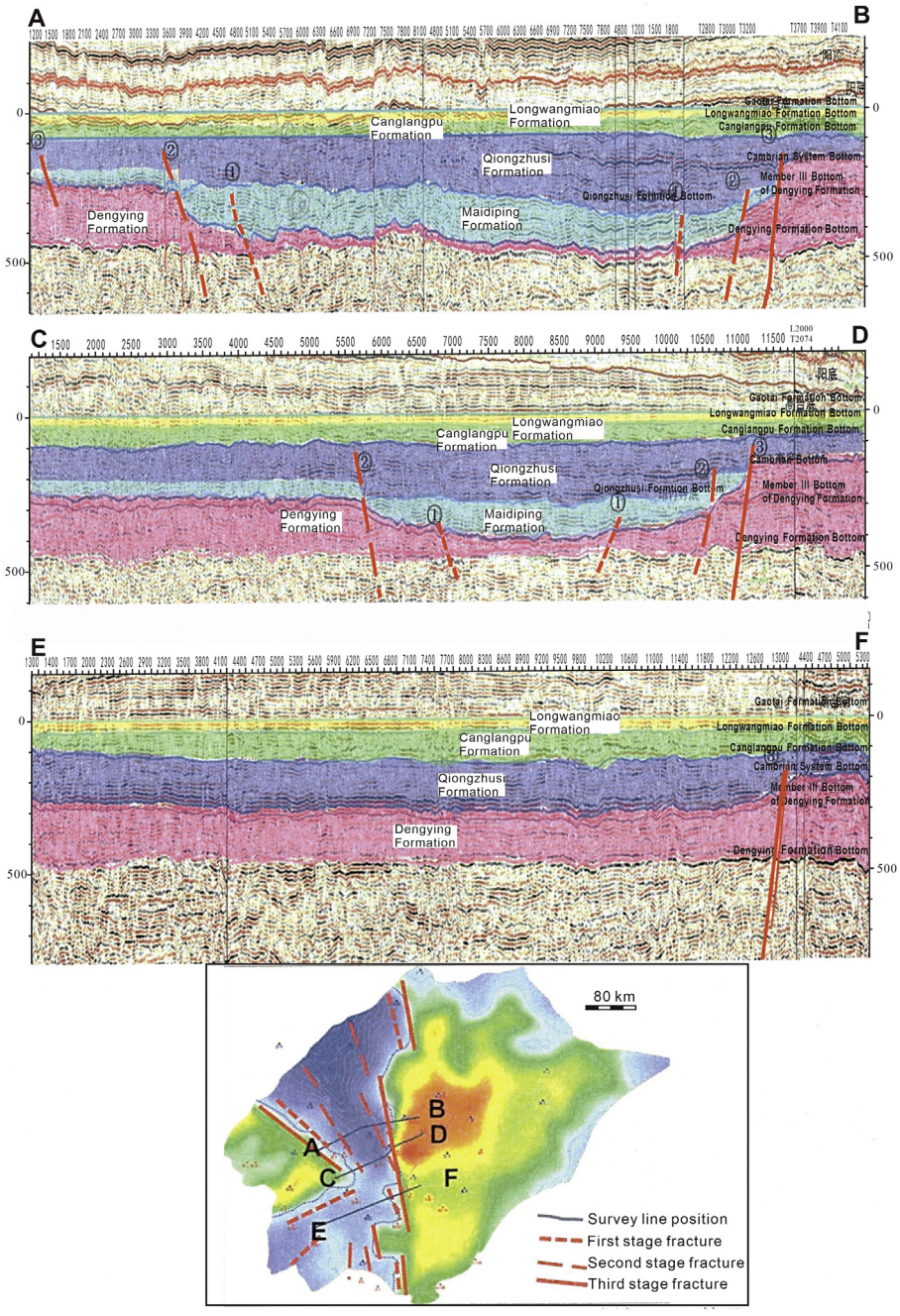

Fig. 14 Seismic profiles (A—B, C—D, and E—F) showing syndepositional faults developed during the Neoproterozoic and Early Paleozoic in Sichuan Basin.

Proterozoic atmosphere were 20—200 times higher than that of modern times (Grotzinger and Knoll, 1995; Kaufman and Xiao, 2003), which may be an important factor affecting the precipitation of the dolostone. Both the previous research results (Pratt, 2001; Kuang *et al.*, 2019) and the recent research results of our relevant teams show that storm deposits are common in the Meso-Neoproterozoic strata of North America, South China, and North China, reflecting the frequent storm climate during this geological period. It is also proved from another side that the Meso-Neoproterozoic platform was in the hot tidal flat-shallow sea environment, and the high temperature of atmosphere is the main reason of frequent storms.

The above analysis indicates that the high concentration of CO_2 in the atmosphere and the frequent hydrothermal recharge of deep faults in the Meso-Neoproterozoic period resulted in the high seawater temperature and high concentration of Mg^{2+}, which

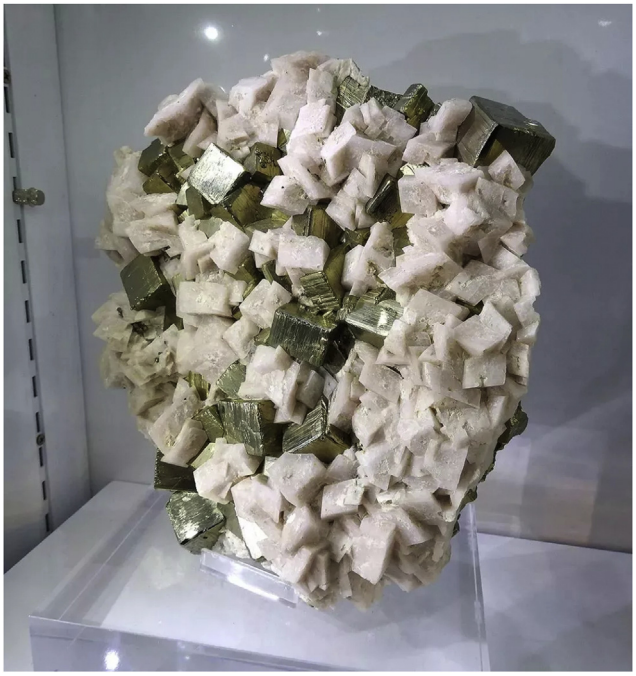

Fig. 15 Symbiotic pyrites with dolostone (from Zhang, 2018).

may be an important driving force for the Mg^{2+} and HCO^{3-} deposition kinetics of primary dolostone. Furthermore, the symbiotic pyrites with dolostone suggest the wide distribution Fe^{2+} in Meso-Neoproterozoic platforms may have catalyzed Mg^{2+} and HCO_3^- to deposited into the primary dolostone (Fig. 15).

Iron ores (magnetite, hematite, pyrites, limonite, and siderite) are widely developed in the Meso-Neoproterozoic strata in China and worldwide, indicating that the seawater at that time was rich in Fe^{2+} ions. Fig. 15 shows the symbiosis of pyrite and dolostone, that is, $CaMg(CO_3)_2$ and FeS_2 precipitate at the same time, indicating that Fe^{2+} ion could be the catalyst for $CaMg(CO_3)_2$ deposition of primary dolostone.

6. Conclusions

The analysis results of petrology, sedimentary environment, and geochemistry indicate that there are large-scale and widely distributed dolostones of typically primary origin in the Meso-Neoproterozoic of platforms of China, including the Upper Ediacaran Qigbulak Formation of the Neoproterozoic in Tarim Basin, the Upper Ediacaran Dengying Formation of the Neoproterozoic in Sichuan Basin, and the Calymmian Wumishan Formation of the Mesoproterozoic in North China Basin. Different types of primary dolostones are all of mud-sized structures (including stromatolite dolostone, oolitic dolostone, and algal laminar dolostone); the microbial dolostone and grain dolostone which were all composed of mud-sized to silt-sized crystallines were deposited in areas with high paleogeomorphology; and the normal mud-sized to silt-sized crystalline dolostones were deposited in the open or restricted platform area. There is no obvious difference in the carbon and oxygen isotopic distribution of dolostone with different sedimentary structures or grain sizes.

All the petrological, sedimentary environmental and geochemical data collectively suggest that the dolostone covering almost whole Meso-Neoproterozoic typical platform areas of China are of relatively typical primary sedimentary origin.

7. Outlook

As the mystery of the origin of dolostone existed for over 250 years, especially the origin mystery of primary dolostone, the preliminary understanding of this study reflects a glimmer of light to solve the mystery. In the future, the research team will further expand the petrology and sedimentology, geochemistry such as Si and Mg isotopes, and fluid inclusion analysis of Meso-Neoproterozoic dolostone, in order to explore and deepen the understanding of the global paleotectonic, paleoclimate, and paleoenvironment of primary dolostone deposition, and to promote the interpretation of genetic mechanism of primary dolostone in basins of China and even around the world.

Authors' contributions

ZDB conceived and designed the paper, HCJ, YW, ZFL, TL, BN, MYW, KL, YQS, HZ wrote the paper, PW, ZLL, ZBY reviewed and edited the manuscript, RL, CXL, XLZ, XQG, PFX, ZXC, SCZ provided datas for this study. All authors read and approved the manuscript.

Funding

Co-funded by the National Key Research and Development Program of China (Nos. 2017YFC 0603104, 2018YF C0604304), Sinopec Group Projects (Nos. 10500000-15-ZC0607-0002, 10500000-18-ZC0607-0003), and China Geological Survey Project (No. IHEGDD2018026).

Conflicts of interest

The authors confirm that they have no competing interests.

Acknowledgements

Thanks to PetroChina Southwest Oil & Gasfield Company, PetroChina Huabei Oilfield Company, PetroChina Tarim Oilfield Company, and Sinopec Star Petroleum Co. Ltd for their strong support in fieldwork and data use. Thanks Prof. Zeng-Zhao Feng and the reviewers for their constructive suggestions on the modification and improvement of the manuscript.

References

Anderson, T.F., Arthur, M.A., 1983. Stable isotopes of oxygen and carbon and their application to sedimentological and paleoenvironmental problems. In: Arthur, M.A., Anderson, T.F., Kaplan, I.R., Veizer, J., Land, L.S. (Eds.), *Stable Isotopes in Sedimentary Geology. SEPM Short Course Notes*, vol. 10, pp. 1—151. https://doi.org/10.2110/scn.83.01.0000.

Bao, Z.D., 1998. Continental slope limestones of Lower and Middle Triassic, South China. *Sedimentary Geology*, 118(1—4), 77—93. https://doi.org/10.1016/S0037-0738(98)00006-2.

Bao, Z.D., 1999. Episodic carbonate deposits on the Triassic continental slope in Southern China. *Acta Geologica Sinica*, 73(1), 93—103. https://doi.org/10.1111/j.1755-6724.1999.tb00815.x.

Bao, Z.D., Chen, J.F., Zhang, S.C., Zhao, H.W., Zhang, Q.H., Li, Y., 2004. Sedimentary environment and development controls of the hydrocarbon source beds: Middle and Upper Proterozoic in northern North China. *Science China Earth Science*, 47(Suppl. II), 133—140. https://doi.org/10.1360/04zd0032.

Bao, Z.D., Jin, Z.J., Sun, L.D., Wang, Z.M., Wang, Q.H., Zhang, Q.H., Shi, X.Z., Li, W., Wu, M.B., Gu, Q.Y., Wu, X.M., Zhang, H.W., 2006. Sea-level fluctuation of the Tarim area in the Early Paleozoic: Respondence from geochemistry and karst. *Acta Geologica Sinica*, 80(3), 366—373. https://doi.org/10.3321/j.issn:0001-5717.2006.03.008 (in Chinese with English abstract).

Bao, Z.D., Li, R.F., Feng, Z.Z., 1999a. Stratigraphic division and correlation of the Ordovician in the eastern and the western Ordos Basin: A review. *Geology Review*, 45(4), 375—381 (in Chinese with English abstract).

Bao, Z.D., Li, R.F., Pang, X.Q., 1999b. Genesis of the massive ordovician dolostones in the Ordos Basin, North China: Evidence from inclusions. *Energy Exploration Exploitation*, 17(3—4), 259—267. https://doi.org/10.1177/014459879901700303.

Bao, Z.D., Qi, Y.C., Jin, Z.J., Zhang, X.L., Hu, G.C., Zhang, Q.H., Shi, X.Z., Li, W., Yang, F., Pan, W.Q., Sun, Y.S., 2007. Karst development respondence to sea-level fluctuation: A case from the Tarim area in the Early Paleozoic. *Acta Geologica Sinica*, 81(2), 205—211. https://doi.org/10.3321/j.issn:0001-5717.2007.02.009 (in Chinese with English abstract).

Bao, Z.D., Zhu, J.Q., Jiang, M.S., Xia, Y., 1998. Isotope and trace element evolution: Responding to sea-level fluctuation — An Example of Ordovician in middle Tarim Basin. *Acta Sedimentologica Sinica*, 16(4), 32—36. https://doi.org/10.14027/j.cnki.cjxb.1998.04.006 (in Chinese with English abstract).

Botz, R.W., von der Borch, C.C., 1984. Stable isotope study of carbonate sediments from the Coorong area, South Australia. *Sedimentology*, 31(6), 837—849. https://doi.org/10.1111/j.1365-3091.1984.tb00890.x.

de Dolomieu, D.G., 1791. Sur un genre de pierres calcaires très peu effervescentes avec les acides et phosphorescentes par la collision. *Journal of Physics*, 39, 3—10.

Du, J.H., Li, X.B., Bao, H.P., Xu, W.L., Wang, Y.T., Huang, J.P., Wang, H.B., Wanyan, R., Wang, J., 2019. Geological conditions of natural gas accumulation and new exploration areas in the Mesoproterozoic to Lower Paleozoic of Ordos Basin, NW China. *Petroleum Exploration Devevelopment*, 46(5), 866—882. https://doi.org/10.1016/S1876-3804(19)60246-6.

Epstein, S., Buchsbaum, R., Lowenstam, H., Urey, H.C., 1951. Carbonate-water isotopic temperature scale. *GSA Bulletin*, 62(4), 417—426. https://doi.org/10.1130/0016-7606(1951)62[417:CITS]2.0.CO;2.

Epstein, S., Buchsbaum, R., Lowenstam, H.A., Urey, H.C., 1953. Revised carbonate-water isotopic temperature scale. *GSA Bulletin*, 64(11), 1315—1326. https://doi.org/10.1130/0016-7606(1953)64[1315:RCITS]2.0.CO;2.

Erez, J., Luz, B., 1983. Experimental paleotemperature equation for planktonic foraminifera. *Geochimica et Cosmochimica Acta*, 47(6), 1025—1031. https://doi.org/10.1016/0016-7037(83)90232-6.

Feng, Z.Z. (Ed.), 1992. *Sedimentary Petrology*. Petroleum Industry Press, Beijing, pp. 64—69 (in Chinese).

Feng, Z.Z. (Ed.), 2004. *Lithofacies Paleogeography of the Cambrian and Ordovician in China*. Petroleum Industry Press, Beijing, pp. 29—47 (in Chinese).

Grotzinger, J.P., Knoll, A.H., 1995. Anomalous carbonate precipitates: Is the precambrian the key to the permian? *Palaios*, 10(6), 578—596. https://doi.org/10.2307/3515096.

He, Y.L., Liu, B., Qin, S., 2010. Study on the dolomitization and dolostone genesis. *Acta Scientiarium Nauralium Universitatis Pekinensis*, 46(6), 1010—1020 (in Chinese with English abstract).

Hebei Bureau of Geology and Mineral Resources Exploration, 1982. *Regional Geological Records of Hebei Province*. Geological Publishing, Beijing, pp. 96—99 (in Chinese).

Horita, J., Zimmermann, H., Holland, H.D., 2002. Chemical evolution of seawater during the Phanerozoic: Implications from the record of marine evaporites. *Geochimica et Cosmochimica Acta*, 66(21), 3733—3756. https://doi.org/10.1016/S0016-7037(01)00884-5.

Huang, S.J., 2010. *Diagenesis of Carbonate Rocks*. Geological Publishing House, Beijing (in Chinese).

Husson, J.M., Higgins, J.A., Maloof, A.C., Schoene, B., 2015. Ca and Mg isotope constraints on the origin of Earth's deepest $\delta^{13}C$ excursion. *Geochimica et Cosmochimica Acta*, 160, 243—266. https://doi.org/10.1016/j.gca.2015.03.012.

Jiang, H.J., Chen, Q.L., Yang, X., Chu, C.L., 2017. The style of sequence stratigraphy of Neoproterozoic rift basin in the Tarim Basin. *Acta Geologica Sinica*, 91(3), 588—604. https://doi.org/10.3969/j.issn.0001-5717.2017.03.007 (in Chinese with English abstract).

Jin, Z.K., Feng, Z.Z., 1999. Origin of dolostones of the Lower Permian in East Yunnan—West Sichuan — Dolomitization through leaching of basalts. *Acta Sedimentology Sinica*, 17(3), 383—389. https://doi.org/10.3969/j.issn.1000-0550.1999.03.008 (in Chinese with English abstract).

Kaufman, A.J., Xiao, S.H., 2003. High CO_2 levels in the Proterozoic atmosphere estimated from analyses of individual microfossils. *Nature*, 425(6955), 279—282. https://doi.org/10.1038/nature01902.

Keith, M.L., Weber, J.N., 1964. Carbon and oxygen isotopic composition of selected limestones and fossils. *Geochimica et Cosmochimica Acta*, 28(10—11), 1787—1816. https://doi.org/10.1016/0016-7037(64)90022-5.

Kuang, H.W., Liu, Y.Q., Geng, Y.S., Bai, H.Q., Peng, N., Fan, Z.X., Song, H.X., Xia, X.X., Wang, Y.C., Chen, X.S., 2019. Important sedimentary geological events of the Meso-Neoproterozoic and their significance. *Journal of Palaeogeography*, 21(1), 1—30. https://doi.org/10.7605/gdlxb.2019.01.001 (in Chinese with English abstract).

Mountjoy, E.W., Halim-Dihardja, M.K., 1991. Multiple phase fracture and fault-controlled burial dolomitization, Upper Devonian Wabamun Group, Alberta. *Journal of Sedimentary Petrology*, 61(4), 590—612. https://doi.org/10.1306/D426776C-2B26-11D7-8648000102C1865D.

Pratt, B.R., 2001. Oceanography, bathymetry and syndepositional tectonics of a Precambrian intracratonic basin: integrating sediments, storms, earthquakes and tsunamis in the Belt Supergroup (Helena Formation, ca. 1.45 Ga), Western North America. *Sedimentary Geology*, 141—142, 371—394. https://doi.org/10.1016/S0037-0738(01)00083-5.

Qian, Y.X., You, D.H., Chen, D.Z., Qing, H.R., He, Z.L., Ma, Y.C., Tian, M., Xi, B.B., 2012. The petrographic and geochemical signatures and implication of origin of the Middle and Upper Cambrian dolostone in eastern margin Tarim: Comparative studies with the Whirlpool point of the Western Canada Sedimentary Basin. *Acta Petrologica Sinica*, 28(8), 2525—2541 (in Chinese with English abstract).

Ren, Y., Zhong, D.K., Gao, C.L., Yang, X.Q., Li, H.Y., Yang, Q., Liu, Y.L., Wang, Y., 2016. Carbon and oxygen isotope compositions and its paleoenvironment implication of Lower Cambrian Longwangmiao Formation in the east part of Sichuan Basin. *Marine and Petroleum Geology*, 21(4), 11—20. https://doi.org/10.3969/j.issn.1672-9854.2016.04.002 (in Chinese with English abstract).

Shackleton, N.J., 1974. *Attainment of Isotopic Equilibrium between Ocean Water and the Benthonic Formainitera Genus Uvigerina: Isotopic Changes in the Ocean during the Last Glacial*, vol. 219. Centre National de la Recherche Scientifique Colloques Internationaux, pp. 203—209.

Sichuan Bureau of Geology, Mineral Resources, 1989. *Regional Geological Records of Sichuan Provience*. Geological Publishing House, Beijing (in Chinese).

Sun, S.Q., 1994. A reappraisal of dolomite abundance and occurrence in the Phanerozoic. *Journal of Sedimentary Research*, A64(7), 360—362.

Taylor, H.P., 1974. The application of oxygen and hydrogen isotope studies to problems of hydrothermal alteration and ore deposition. *Economic Geology*, 69(6), 843—883. https://doi.org/10.2113/gsecongeo.69.6.843.

Timofeeff, M.N., Lowenstein, T.K., Da Silva, M.A.M., Harris, N.B., 2006. Secular variation in the major-ion chemistry of seawater: Evidence from fluid inclusions in Cretaceous halites. *Geochimica et Cosmochimica Acta*, 70(8), 1977—1994. https://doi.org/10.1016/j.gca.2006.01.020.

Tucker, M.E., 1982. Precambrian dolomites: Petrographic and isotopic evidence that they differ from Phanerozoic dolomites. *Geology*, 10(1), 7—12.

Turner, E.C., 2009. Mesoproterozoic carbonate systems in the borden basin, Nunavut. *Canadian Journal of Earth Science*, 46(12), 915—938. https://doi.org/10.1139/E09-062.

Vasconcelos, C., McKenzie, J.A., Bernasconi, S., Grujic, D., Tiens, A.J., 1995. Microbial mediation as a possible mechanism for natural dolomite formation at low temperatures. *Nature*, 377(6546), 220—222. https://doi.org/10.1038/377220a0.

Veizer, J., Ala, D., Azmy, K., Bruckschen, P., Buhl, D., Bruhn, F., Carden, G.A.F., Diener, A., Ebneth, S., Godderis, Y., Jasper, T., Korte, C., Pawellek, F., Podlaha, O.G., Strauss, H., 1999. $^{87}Sr/^{86}Sr$, $\delta^{13}C$ and $\delta^{18}O$ evolution of Phanerozoic seawater. *Chemical Geology*, 161(1—3), 59—88. https://doi.org/10.1016/S0009-2541(99)00081-9.

von der Borch, C.C., 1976. Stratigraphy and formation of Holocene dolomitic carbonate deposits of the Coorong area, South Australia. *Journal of Sedimentary Petrology*, 46(4), 952—966. https://doi.org/10.1306/212F709F-2B24-11D7-8648000102C1865D.

Wang, D., 2017. *Tectonic Paleogeographic Evolution and Petroleum Geological Significance during Late Spinian—Early Cambrian in Central Sichuan Basin* (Ph.D. Thesis). Yangtze University, Wuhan, p. 76 (in Chinese).

Warren, J., 2000. Dolomite: Occurrence, evolution and economically important associations. *Earth Science Review*, 52(1—3), 1—81. https://doi.org/10.1016/S0012-8252(00)00022-2.

Wei, G.Q., Zhu, Q.Y., Yang, W., Zhang, C.L., Mo, W.L., 2019. Cambrian faults and their control on the sedimentation and reservoirs in the Ordos Basin, NW China. *Petroleum Exploration Development*, 46(5), 883—895. https://doi.org/10.1016/S1876-3804(19)60247-8.

Wei, X., Zhu, Y.J., Xu, H., Zhao, G.C., Li, Y.X., 2006. Discussion on Neogene dolostone forming condition in

Xisha Islands: Evidences from isotope C and O and fluid inclosures. *Acta Petrologica Sinica*, 22(9), 2394—2404. https://doi.org/10.3321/j.issn:1000-0569.2006.09.016 (in Chinese with English abstract).

White, B., 1981. Shallowing-upward cycles in the Middle Proterozoic Altyn Formation. *Nature*, 294(5837), 157—158. https://doi.org/10.1038/294157a0.

Wood, R., Liu, A.G., Bowyer, F., Wilby, P.R., Dunn, F.S., Kenchington, C.G., Cuthill, J.F.H., Mitchell, E.G., Penny, A., 2019. Integrated records of environmental change and evolution challenge the Cambrian Explosion. *Nature Ecology Evolution*, 3(4), 528—538. https://doi.org/10.1038/s41559-019-0821-6.

Wu, L., Guan, S.W., Yang, H.J., Ren, R., Zhu, G.Y., Jin, J.Q., Zhang, C.Y., 2017. The paleogeographic framework and hydrocarbon exploration potential of Neoproterozoic rift basin in northern Tarim Basin. *Acta Pet. Sin.*, 38(4), 375—385. https://doi.org/10.7623/syxb201704002 (in Chinese with English abstract).

Xinjiang Bureau of Geo-Exploration, Mineral Development, 1993. *Regional Geological Records of Xinjiang Uygur Autonomous Region*. Geological Publishing House, Beijing (in Chinese).

Yang, F., Bao, Z.D., Zhang, D.M., Jia, X., Xiao, J., 2017. Carbonate secondary porosity development in a polyphase paleokarst from Precambrian system: Upper Sinian examples, North Tarim Basin, Northwest China. *Carbonates Evaporites*, 32(2), 243—256. https://doi.org/10.1007/s13146-017-0336-7.

Zenger, D.H., Dunham, J.B., Ethington, R.L., 1980. Concepts and models of dolomitization. *SEPM Special Publication*, 28, 320. https://doi.org/10.2110/pec.80.28.

Zhang, D.M., Bao, Z.D., Pan, W.Q., Hao, Y., Chen, Y.Q., Wang, J., Zhang, Y.Q., Lai, H.F., 2014. Characteristics and forming mechanisms of evaporite platform dolomite reservoir in Middle Cambrian of Xiaoerbulake section, Tarim Basin. *Natural Gas Geoscience*, 25(4), 498—507. https://doi.org/10.11764/j.issn.1672-1926.2014.04.0498 (in Chinese with English abstract).

Zhang, Z., 2018. *The Wonderful Stone: Pyrite Dolomite. 6th China (Hunan) International Mineral & Gem Expo, Chenzhou* (in Chinese).

Zhao, C.L., Xu, Y.K., Bai, G.Y., Lai, X.K., 1977. Sedimentary characteristics and facies analysis of the Gaoyuzhuang formation-Wumishan Formation in the North-central Taihang mountains. *Journal of East China Petroleum Institute*, 1(3), 118—138 (in Chinese).

Zhao, C.L., Zhu, X.M., 2001. *Sedimentary Petrology*, the third ed. Petroleum Industry Press, Beijing (in Chinese).

Zhu, J.Q., Zhang, Y.S., Yu, B.S., Wu, S.Q., You, X.L., Liu, L., He, K., 2013. Dolomite. In: Feng, Z.Z. (Ed.), *Sedimentology of China*, the second ed. Petroleum Industry Press, Beijing, pp. 266—331 (in Chinese).

Zhu, M.Y., 2016. Research progress of global Neoproterozoic sedimentary strata. In: Sun, S., Wang, T.G. (Eds.), *Middle Neoproterozoic Geology and Oil and Gas Resources in Eastern China*. Science Press, Beijing, pp. 3—24 (in Chinese).